Winter 2021

Geologic Mapping along the Benton Spring Fault, Nevada: Dextrally-offset Tuff-filled Paleovalleys in the Central Walker Lane

Peter Dubyoski
Central Washington University

GEOLOGIC MAPPING ALONG THE BENTON SPRING FAULT, NEVADA: DEXTRALLY-OFFSET TUFF-FILLED PALEOVALLEYS IN THE CENTRAL WALKER LANE

_____

A Thesis

Presented to

The Graduate Faculty

Central Washington University

_____

In Partial Fulfillment

of the Requirements for the Degree

Master of Science

Geological Sciences

_____

by

Peter Brent Dubyoski Jr.

March 2021

CENTRAL WASHINGTON UNIVERSITY

Graduate Studies

We hereby approve the thesis of

Peter Brent Dubyoski Jr.

Candidate for the degree of Master of Science

APPROVED FOR THE GRADUATE FACULTY

_____ _____
Dr. Jeffrey Lee, Committee Chair

_____ _____
Dr. Wendy A. Bohrson

_____ _____
Dr. Chris Mattinson

_____ _____
Dean of Graduate Studies

ABSTRACT

GEOLOGIC MAPPING ALONG THE BENTON SPRING FAULT, NEVADA:

DEXTRALLY-OFFSET TUFF-FILLED PALEOVALLEYS

IN THE CENTRAL WALKER LANE

by

Peter Brent Dubyoski Jr.

Documenting the spatiotemporal evolution of fault systems along the western margin of North America is a prerequisite for characterizing the forces which drive faulting across the U.S. Cordillera. Within the Cordillera, the Walker Lane, characterized by active intracontinental faults, straddles the western edge of the Basin and Range Province and the eastern edge of the Sierra Nevada. In the Gabbs Valley Range, central Nevada, eastern Central Walker Lane, I combine new mapping, geochronology, and structural studies to document the geometry and timing of dextral fault slip along the Benton Spring fault, an active intracontinental fault. The Benton Spring fault is one of four major dextral faults in the region; my studies provide insight into this fault's late Oligocene and Miocene fault slip history. Utilizing the walls of a series of inset volcanic rock infilled paleovalleys, which are preserved in the Gabbs Valley Range, I identified five markers dextrally offset across the Benton Spring fault. Previous studies provided ages for three of the volcanic units which infill these paleovalleys, while my new geochronology provides ages for a further two. All five markers record, within error, the same magnitude of dextral offset, indicating that the average

dextral offset of 6.9 ± 1.5 km accumulated after the emplacement of the youngest dated volcanic unit at 20.14 ± 0.26 Ma. The adjacent Petrified Spring fault records similar magnitude of dextral offset, and azimuth and timing of fault slip as the Benton Spring fault; I assume that similar forces drove initiation of slip along both faults and thus slip likely initiated at the same time. Initiation of dextral slip along the major dextral faults of the eastern Central Walker Lane is constrained to the Middle Miocene as is initiation of slip along the normal faults bounding the eastern flank of the Sierra Nevada and within the Basin and Range. Given the close spatial-temporal relationship of the two different fault types, I suggest the same forces drove both normal and strike-slip faulting.

ACKNOWLEDGEMENTS

I would like to acknowledge Zac Bales for his exceptional field assistance. I would also like to thank Dean Miller, James Saburomaru, and Katie Sullivan at the USGS Menlo Park facility for their assistance in mineral separation and sample preparation for irradiation. Additional thanks to Anne Egger for her guidance in preparation of base maps and other GIS utilization. Primary funding for this project was provided by the U.S. Geological Survey, National Cooperative Geologic Mapping Program, grant G15AC00171, awarded to J. Lee. Additional funding was provided by a National Science Foundation Grant, EAR-1419808, awarded to J. Lee. Stereonet plots were produced using Stereonet 9.9.3 software thanks to Rick Allmendinger.

I would like to dedicate this work to Moriah Kauer and Kevin DeLano. Moriah provided both support and advice when this work stretched beyond its planned timeline, and without Kevin's check-in calls and advice I doubt that this document would ever have been completed.

TABLE OF CONTENTS

LIST OF TABLES

LIST OF FIGURES

LIST OF FIGURES (CONTINUED)

CHAPTER I

INTRODUCTION

The Mesozoic-Cenozoic Pacific-North American plate boundary records the transition from an Andean-style subduction margin to a transform boundary (e.g. Atwater and Stock, 1998; DeMets and Merkourkiev, 2016). The subduction and fragmentation of the Farallon plate at ~28 Ma resulted in the contact between the Pacific and North American plates, resulting in the onset of the transform slip along this plate boundary (Atwater and Stock, 1998) (Figure 1). The contact between the Pacific and North American plates has lengthened since 28 Ma as the Farallon plate was further fragmented and the resulting microplates either subducted beneath the North American plate or were captured by the Pacific plate (Atwater and Stock, 1998) (Figure 1). Reconstructions of the Pacific-North American transform plate boundary since 20 Ma indicate a ~70% increase in relative motion from 19.7 to 9 ± 1 Ma and a subsequent rate of motion which varied by less than ± 2 percent (DeMets and Merkouriev, 2016). Modern plate boundary strain is primarily accommodated along the San Andreas fault system, with ~20-25% of that strain being distributed east of the Sierra Nevada in the Walker Lane (e.g. Dixon et al., 1995; Bennett et al., 2003; Faulds and Henry, 2008; Lee et al., 2009; Delano et al., 2019) (Figure 1).

The Walker Lane is a zone of dextral shear defined by a system of dominantly NW-striking strike-slip faults; the zone ranges from 25 to 130 km in width and extends northward from the Mojave Desert along the eastern flank of the Sierra Nevada, overlapping with the western edge of the Basin and Range (e.g., Stewart, 1988; Dokka

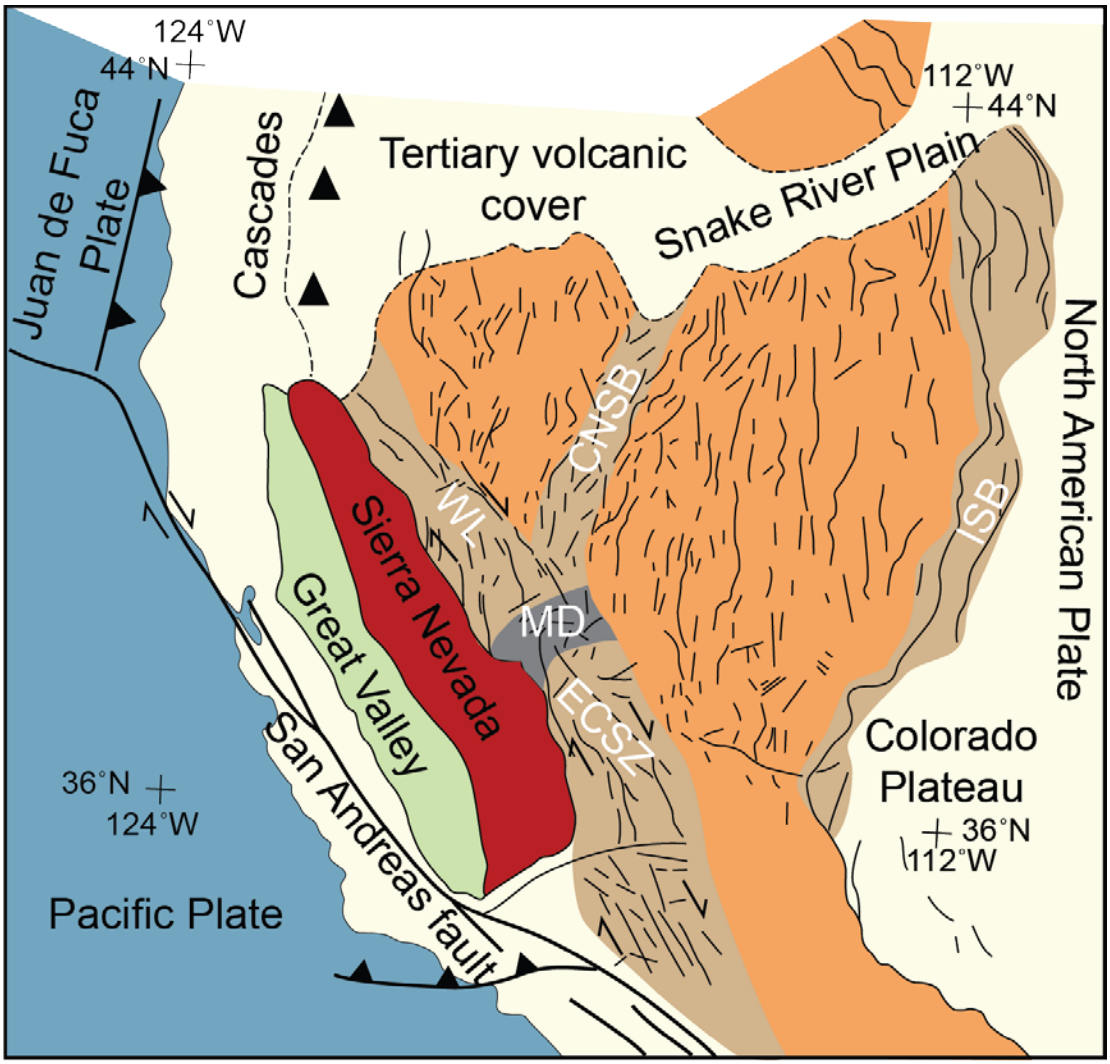

Figure 1. Simplified tectonic map of the western part of the US Cordillera showing the major tectonic provinces and plate boundaries. Basin and Range province is in orange; CNSB (Central Nevada Seismic Belt), ECSZ (Eastern California Shear Zone), ISB (Intermountain Seismic Belt), and WLB (Walker Lane Belt) are in lightbrown. MD (Mina Deflection) is in dark grey. Sierra Nevada is in red and Great Valley is in green. Modified from Lee et al., 2020

and Travis, 1990; Dixon et al., 1995; Bennett et al., 2003; Faulds and Henry, 2008) (Figure 1 and 2). Displacement is recorded earlier in the southern Walker Lane than in the northern Walker Lane, suggesting that, like the San Andreas fault, the Walker Lane has been propagating northward (e.g. Atwater and Stock, 1998; Faulds et al., 2005; DeMets and Merkouriev, 2016). Unlike the San Andreas fault system, which comprises a series of extensive, interconnected dextral faults several hundred kilometers in length (e.g., Powell et al., 1993), the Walker Lane comprises a system of discontinuous en echelon dextral faults kinematically linked by sinistral faults and normal faults (e.g. Faulds and Henry, 2008; Delano et al., 2019) (Figure 2). Due to the greater number of faults, their geometric complexity, and geographic distribution across the Walker Lane, geologic slip rates along the many of faults of the Walker Lane are not well constrained.

This study aims to provide new constraints on the geometry and magnitude of offset, timing of initiation of slip, and geologic slip rates along the Benton Spring fault, a dextral fault in the eastern Central Walker Lane (Figure 2). The Central Walker Lane is a ~130-km-wide dextral shear zone bounded by the Sierra Nevada to the west, the sinistral faults of the Mina deflection and Carson domain to the south and north, respectively, and Basin and Range extensional faults to the east (e.g., Faulds and Henry, 2008; Bormann et al., 2016) (Figure 2). The eastern Central Walker Lane comprises the eastern portion of the Central Walker Lane, bounded to the west by the Wassuk Range (e.g., Bormann et al., 2016) (Figure 3). Strain in the eastern Central Walker Lane is primarily accommodated along four major and two minor dextral faults which pass through the Gillis and Gabbs Valley Ranges (Wesnousky, 2005; Lee et al., 2020b) (Figure 3). The

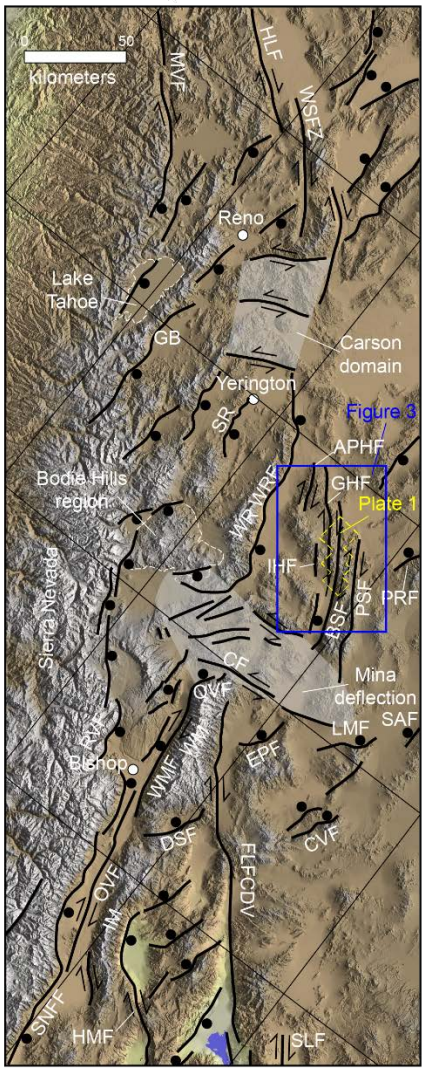

Figure 2. Shaded relief map of the Walker Lane showing location of major Quaternary faults, the Carson Domain, the Mina Deflection, the Bodie Hills region. Solid blue box shows the location of Figure 3 and the dashed yellow polygon shows the location of the geologic map in Plate 1. Solid ball is located on the hanging wall of normal faults; arrow pairs indicate relative motion across strike-slip faults.

Fault abbreviations (alphabetical):
AH, Anchorite Hills fault zone;
APHF, Agai Pai Hills fault;
BSF, Benton Springs fault;
CF, Coaldale fault;
CVF, Clayton Valley fault;
FCDV, Fish Lake Valley-Furnace Creek-Death Valley fault zone
GHF, Gumdrop Hills fault;
HLF, Honey Lake fault;
HMF, Hunter Mountain fault;
IHF, Indian Head fault;
LMF, Lone Mountain fault;
MVF, Mohawk Valley fault;
OVF, Owns Valley fault;
PSF, Petrified Springs fault;
QVF, Queen Valley fault;
RVF, Round Valley fault;
SAF, San Antonio Mountains range front fault;
SLF, Stateline fault;
SNFF, Sierra Nevada frontal fault zone;
TPF, Towne Pass fault;
WMF, White Mountains fault zone;
WRF, Wassuk Range fault;
WSFZ, Warm Springs fault zone.

Modified from Lee et al., 2020

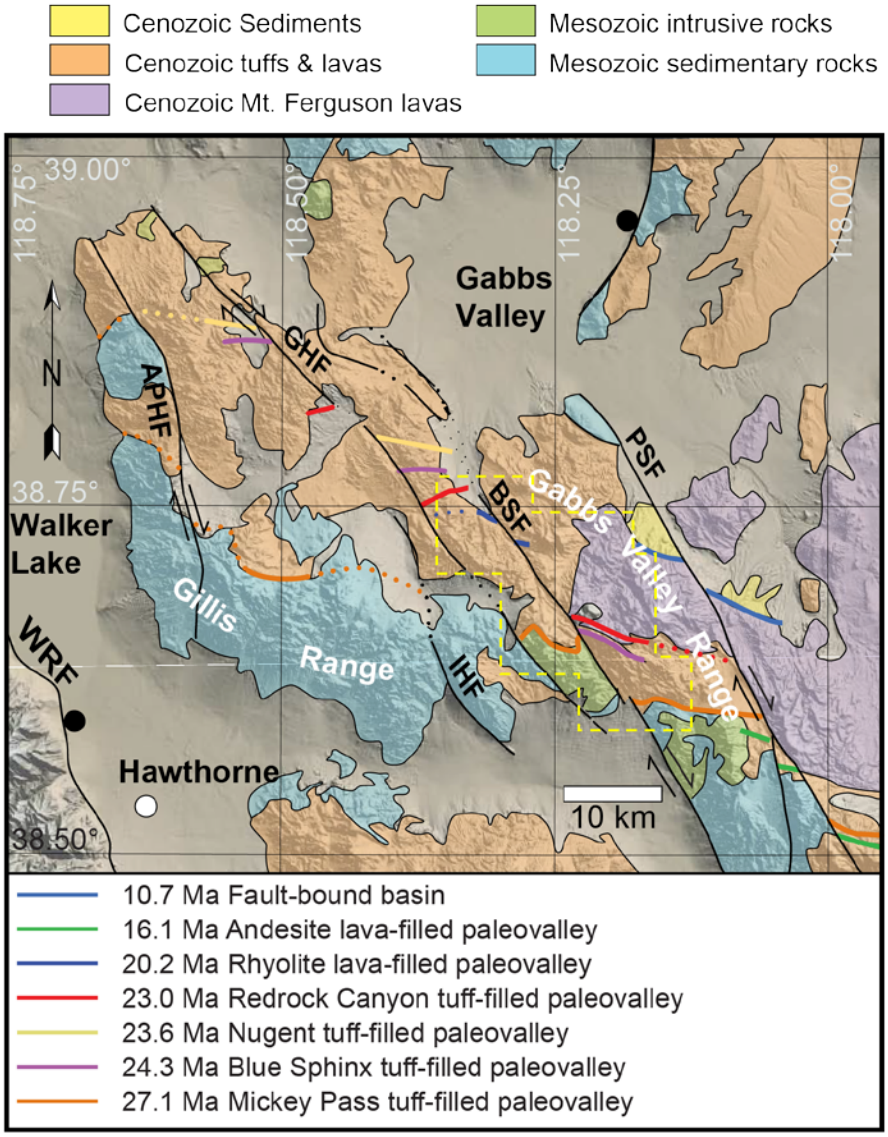

Figure 3. Shaded-relief map of the Central Walker Lane Belt showing the major Cenozoic faults and documented (solid lines) and postulated (dotted lines) volcanic-filled paleovalleys and other dextrally offset markers. Location of the Benton Spring field area (Plate 1) shown with dashed yellow polygon. Fault abbreviations not defined in Figure 1: APHF, Agai Pah Hills fault; IHF, Indian Head fault. See Figure 2 for location of map, additional fault abbreviations, and definition of fault symbols. Modified from Hoxey et al. (2018) and Lee et al. (2020). Reported ages, which are approximate, from Evernden et al. (1964), Henry and John (2013), Henry and Faulds (2010), Lee et al. (2020).

Benton Spring fault runs through the Gabbs Valley Range, where underlying Mesozoic sedimentary and intrusive rocks are nonconformably overlain by Cenozoic volcanic and sedimentary rocks (Hardyman, 1980; Ekren et al., 1980; Ekren and Byers, 1985a, 1985b, 1985c, 1985d; Hoxey et al., 2020; Lee et al., 2020b).

To constrain the slip history of the Benton Spring fault, I test two primary hypotheses. The first hypothesis is that the Cenozoic volcanic and sedimentary rocks in the Gabbs Valley Range fill paleovalleys incised into the Mesozoic bedrock and Cenozoic rocks and that the walls and other features of these paleovalleys can be used as geologic markers to determine the magnitude of dextral offset across the Benton Spring fault. To test this hypothesis, I completed new geologic mapping and structural studies along the 25-km long map trace of the Benton Spring fault in the Gabbs Valley Range (Figure 2, 3) (Plates 1, 2, and 3). The second hypothesis is that the slip rate along the Benton Spring fault varies through time. To test this hypothesis, I collected samples from volcanic units that in-filled dextrally offset paleovalleys in the Gabbs Valley Range for $^{40}Ar/^{39}Ar$ geochronology to determine the emplacement ages of lavas and tuffs. The ages of the emplaced volcanic rocks, coupled with the magnitude of dextral offset for each associated geologic marker, allows for calculation of the average slip rates for the Benton Spring fault since the emplacement of each dated rock unit. The new data I collected to explore these two hypotheses, combined with published fault slip data across the Central Walker Lane, provides a basis to address a more complex question: what is the spatial-temporal distribution of dextral fault slip across the eastern Central Walker Lane? In addition, comparing the timing of dextral fault slip for the Benton Spring fault and

published dextral slip in the rest of the eastern Central Walker Lane (Lee et al., 2020b) allows an examination of the development of this region in the context of Basin and Range faulting and the forces that drive this intracontinental faulting.

CHAPTER II

LITERATURE REVIEW

Walker Lane Tectonics

Geodetic studies suggest that the Pacific Plate is moving northwest at rate of ~50 mm/yr relative to the North American Plate (e.g. Demets and Dixon, 1999; Dixon et al., 2000, 2003; Bennett et al., 2003; DeMets and Merkouriev, 2016). Approximately 75% of this motion is accommodated along the San Andreas Fault system (Freymueller et al., 1999; Savage et al., 2004). Approximately 80% of the remaining ~13 mm/yr motion is distributed throughout the Eastern California Shear Zone and the Walker Lane in western Nevada and eastern California (e.g. Bennett et al., 2003). The Walker Lane is a zone of dominantly NW-striking dextral faults extending north from the Garlock fault in southern California to the California Modoc plateau (e.g. Stewart, 1988; Faulds and Henry, 2008).

Dextral shear is accommodated along dominantly northwest-striking strike-slip faults in the Central Walker Lane, the portion of the Walker Lane exposed between the Mina Deflection to the south and the Carson domain to the north (e.g. Cashman and Fontaine, 2000; Wesnousky, 2005; Nagorsen-Renke et al., 2013) (Figure 2). Strain is transferred from the approximately east-west-striking sinistral faults of the Mina deflection into the Central Walker Lane and from there to the northern Walker Lane (e.g. Wesnousky, 2005; Delano et al., 2019).

Based on new interseismic GPS velocities and continuous GPS networks monitoring deformation of the Pacific-North America plate boundary, Bormann et al. (2016) calculated a deformation budget of ~8 mm/yr across the Central Walker Lane. The

difference in deformation budgets between previous GPS studies (e.g. Oldow et al., 2001; Bennett et al., 2003) and Bormann et al.'s (2016) study is the result of correction for postseismic relaxation following large magnitude earthquakes across the Central Nevada Seismic Belt earthquakes (Hetland, 2003; Gourmelen and Amelung, 2005; Hammond et al., 2009; Bormann et al., 2016) (Table 1).

TABLE1. MAJOR CENTRAL NEVADA SEISMIC BELT EARTHQUAKES

Location	Date	Latitude	Longitude	Magnitude	Source
Pleasant Valley	3 October 1915	40.5	-117.5	7.6	Doser (1988)
Cedar Mountain	21 December 1932	38.80	-117.98	7.2	Abe (1981)
Fairview Peak	16 December 1954	39.20	-118.00	7.2	Doser (1986)
Dixie Valley	16 December 1954	39.67	-117.87	6.8	Doser (1986)

Central Walker Lane

My field area, located in the Gabbs Valley Range, falls within the eastern Central Walker Lane and is centered on the Benton Spring fault. Across the eastern Central Walker Lane, the majority of dextral motion is accommodated along five major strike-slip faults spaced between 3 and 10 km apart; the faults are, from west to east, the Agai Pai Hills, the Indian Head, the Gumdrop Hills, the Benton Spring, and the Petrified Spring faults (Figure 3).

The Benton Spring fault is the primary fault examined in this study. Assessments of the total length of the fault range from 50 km to 95 km (Ekren and Byers, 1984; Hardyman, 1984), with the USGS Quaternary Fault and Fold Database of the United States listing a length of 87 km (Sawyer, 1998a). Multiple Holocene earthquakes have occurred along the Benton Spring fault with estimated maximum magnitudes of M_w ~6.8 and a recurrence interval of 1,600 – 2,300 years (Angster et al., 2019). Of the six faults of

the eastern Central Walker Lane, the Benton Spring fault records the most recent recognized surface-rupturing event, which occurred approximately 800 years ago (Langille et al., 2018; Angster et al., 2019).

Mapping of the northern terminus of the Benton Spring fault in the Terrill Mountains (Carlson, 2018) identified an Oligocene paleosol dextrally offset ~6 km across the fault. This paleosol underlies the Tuff of Toiyabe dated at 23.29 ± 0.02 Ma and overlies an older Oligocene tuff of unknown age; this tuff in turn unconformably overlies the Tuff of Gabbs Valley, dated to 24.95 ± 0.02 Ma (Carlson, 2018). Dextral slip along the section of the Benton Spring fault exposed in the Terrill Mountains is therefore constrained to a maximum initiation age of 24.95 ± 0.02 Ma. Carlson (2018) notes that the trace of the Benton Spring fault at its northern terminus is more curvilinear than elsewhere in the Central Walker Lane; this change in strike was interpreted as a possible indication of strain partitioning to dextral faults obscured beneath Quaternary sediments on Rawhide Flat to the northeast.

To the south of the Gabbs Valley Range, the Benton Spring fault can be traced at the base of the western edge of the Pilot Mountains (Oldow and Meinwals, 1992; Oldow and Dockery, 1993, Bell, 1995). A lack of offset markers along this trace of the fault precluded assessment of the style and timing of fault slip. It is unclear whether the Benton Spring fault continues farther south and acts as a range-bounding fault for the Monte Cristo Range; the southernmost mapped fault traces attributed to the Benton Spring fault are located near the mouth of Long Canyon south of the Pilot Mountains (Dohrenwend, 1982). On the western margin of the Monte Cristo Range, several normal

faults strike parallel to the western boundary of the range, and sub-parallel to the southernmost mapped trace of the Benton Spring fault in the Pilot Range; to the south the map traces of these faults terminate just north of the Coaldale fault (Dohrenwend et al., 1996) It is unclear whether these faults represent a portion of the Benton Spring fault or are unassociated with the Benton Spring fault.

An elastic block model of Central Walker Lane GPS velocities yielded a dextral slip rate of 0.98 ± 0.36 mm/yr for the Benton Spring fault, 0.58 ± 0.47 mm/yr for the Petrified Spring fault, and 0.47 ± 0.14 mm/yr for the Indian Head fault (Bormann et al., 2016). The 78 fault trains used to define boundaries for the 35 blocks in the Bormann et al. (2016) model represented a simplification of known Quaternary active faults; the major faults of the eastern Central Walker Lane were simplified to three fault trains along the map traces of the aforementioned faults. The model slip rates for the Petrified Spring and Benton Spring faults comprise the majority of the 2.7 ± 0.7 mm/yr of slip accommodated across the Gabbs Valley and Gillis Ranges (Bormann et al., 2016).

Offset Markers and Magnitudes

Early work assessing dextral offset across the Benton Spring fault yielded a range of estimates: Ekren and Byers (1984) suggested 6-10 km based on offset of a Cretaceous granite pluton and 8 km based on the Cenozoic Nugent tuff, while Stewart (1988) matched the southern limit of Cenozoic tuffs east and west of the Benton Spring fault yielding 5-6 km of offset.

CHAPTER III

GEOLOGIC ROCK UNITS AND AGES IN THE BENTON SPRING FIELD AREA

Based on field mapping at the 1:12,000 scale of a ~230 km^2 area straddling the central section of the Benton Spring fault, Gabbs Valley Range (Plate 1), I separate geologic units in the field area into Mesozoic, Oligocene, Miocene, Pliocene, and Quaternary phases (Plate 2). Below, I briefly describe the map units used in the geologic map of Plate 1, which encompasses the field area of the study. Detailed descriptions of pre-Quaternary map units can be found in Plate 2. The Mesozoic basement rock is composed of sedimentary, metasedimentary, and intrusive igneous rocks and is unconformably overlain by Cenozoic paleosols, Oligocene to Miocene tuffs, fluvial gravels, lava flows, and lacustrine deposits. Many of these units appear to fill a primary paleovalley incised into the Mesozoic basement (Figure 4). Pliocene alluvial and colluvial deposits lie unconformably atop the Oligocene and Miocene volcanic and sedimentary sequence, and Quaternary sedimentary deposits lying unconformably atop older units represent the youngest units in the field area (Plates 1, 2, and 3). Locally, the combination of areal distribution of volcanic rocks, geometry of contacts, range of lithologies exposed, and orientation of volcanic structures indicates that five NW-SE to E-W trending paleovalleys are nested within the primary NW-SE trending paleovalley incised into the basement rocks. All pre-Quaternary units, and the infilled paleovalleys, are dextrally offset by the NNW-striking Benton Spring fault.

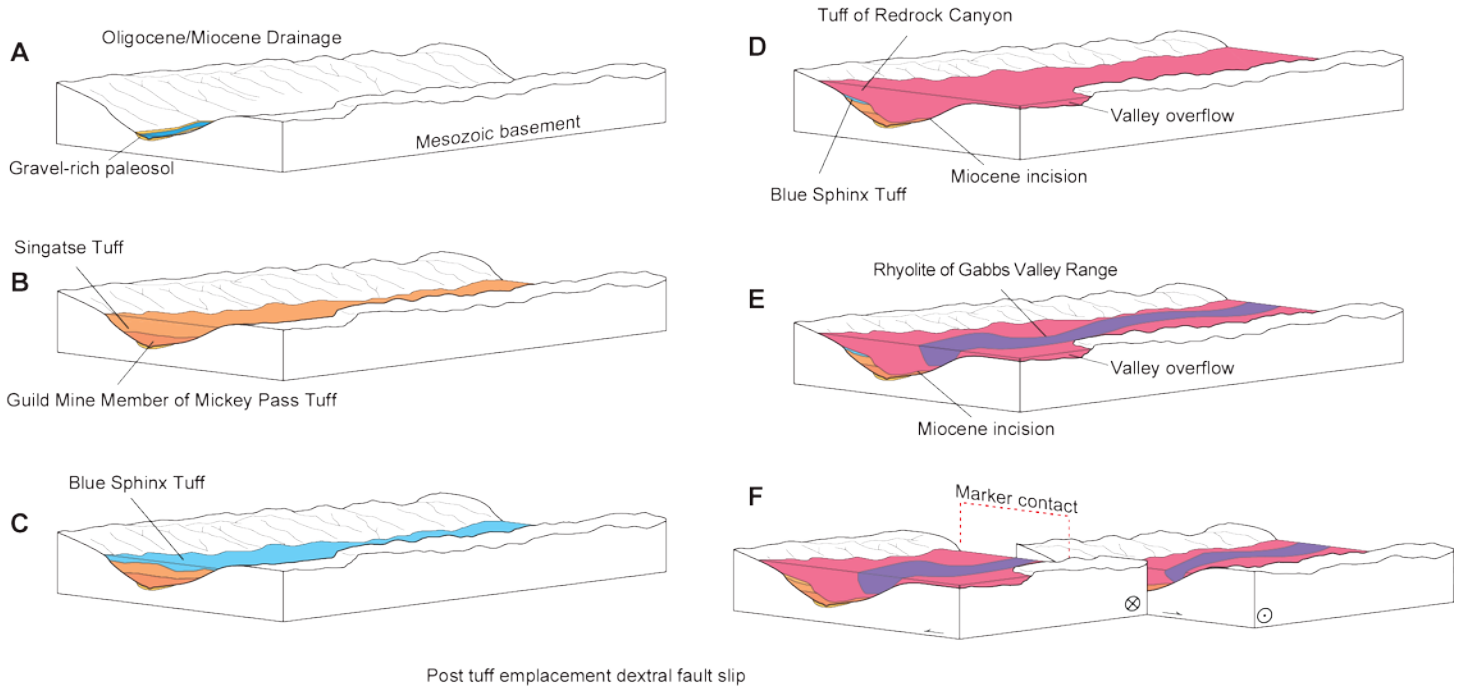

Figure 4. Schematic block model representation of paleovalley evolution and later faulting. (A) Early Cenozoic valley incision and gravel-rich paleosol development on Mesozoic basement. (B) Emplacement of Guild Mine Member of the Mickey Pass Tuff and Singatse Tuff. (C) Continued incision and emplacement of Blue Sphinx Tuff. (D) Continued Incision and emplacement of Tuff of Redrock Canyon with overflow. (E) Incision and emplacement of Rhyolite of Gabbs Valley Range, creating two apparent channels of Tuff of Redrock Canyon. (F) Paleovalley walls act as geologic marker across dextral fault. Modified from Lee et al. (2020).

Mesozoic Units

The Mesozoic basement is comprised of the Triassic Luning Formation (Ekren and Byers, 1985a), Triassic crystalline limestone (Trli), Jurassic diorite and granodiorite, and Cretaceous-Jurassic granite (Plate 2). The Cretaceous-Jurassic granite intrudes older Mesozoic units. This granite generally forms the base of the primary paleovalley and is locally overlain by a Mesozoic-Cenozoic paleosol consisting of strongly weathered, decomposed granite, granite core stones, and grus (Figure 5b) that is interpreted as evidence of long-term exposure.

Oligocene Units

Oligocene rocks in the field area consist of welded ash-flow tuffs and deposits comprised of altered or brecciated byproducts of these tuffs (Plate 2). These tuffs are generally confined to paleovalleys throughout the field area and the source calderas have been located to the east of the field area (Proffett and Proffett, 1976, Templeton 1998, Henry 2008, Henry and John 2013).

Nonconformably overlying the Mesozoic basement rock is the oldest observed Oligocene unit, the Guild Mine Member of the Mickey Pass Tuff (Obmg). The exposed contact between the Mickey Pass Tuff and Mesozoic units is generally high-angle and is frequently marked by the presence of the aforementioned paleosol, grus, and corestones. Outcrops frequently exhibit evidence of extensive hydrothermal alteration. The unit has an interpreted eruptive volume of 600 km^3 (Proffett and Proffett, 1976, Templeton 1998). Sanidine from this unit yielded an $^{40}Ar/^{39}Ar$ age of 27.28 ± 0.02 Ma (Henry and John, 2013).

Nonconformably overlying the Guild Mine Member of the Mickey Pass Tuff is the Singatse Tuff (Obsi) (Plates 1 and 2). The basal portion of the Singatse Tuff is dark purple and outcrops directly atop the Guild Mine Member of the Mickey Pass Tuff in the southern portion of the field area. Elsewhere, the Singatse Tuff is in near vertical contact with the older Obmg (Figure 4b). Some exposures of the Singatse Tuff west of the Benton Spring fault exhibit extensive silicification and argillization, indicating extensive hydrothermal alteration. The Singatse Tuff is also a large-volume pyroclastic flow deposit found throughout Nevada and has an interpreted eruptive volume of 3500 km^3 (e.g. Proffett and Proffett, 1976). Sanidine from the Singatse Tuff yielded an $^{40}Ar/^{39}Ar$ age of 26.85 ± 0.02 Ma (Henry and John, 2013).

Lying unconformably atop, and in some cases banking against, the Singatse Tuff and locally lying atop a dark-grey fluvial gravel is the Blue Sphinx Tuff (Osp) (Plates 1 and 2; Figure 4c). The fluvial gravel (too thin to map as an individual unit) contains clasts up to 10 cm in diameter of both the Guild Mine Member of the Mickey Pass Tuff and the Singatse Tuff. In the field area the Blue Sphinx Tuff exhibits extensive hydrothermal alteration in nearly all outcrops. The Blue Sphinx Tuff has a thickness of up to 100 m in the field area and records a sanidine $^{40}Ar/^{39}Ar$ age of 24.30 ± 0.05 Ma (Henry and John, 2013).

Unconformably overlying the Blue Sphinx Tuff and other Oligocene units are a series of rhyodacite flows, the Lavas of Nugent Wash (Mln) (Plates 1 and 2). Mapped as a single unit, this series of lava flows ranges from dark red to dark brown with visible flow banding (Plates 1 and 2).

Unconformably overlying the lavas of Nugent Wash is the Nugent Tuff (Mhn), a series of ash-flow tuff deposits that were not distinguishable in the field, and as such were mapped as a single unit (Plates 1 and 2). Ash-fall tuff deposits were frequently observed between the different ash-flow deposits, but correlation between outcrops proved impossible in the field.

A hornblende-rich andesite (Ola) outcrops with high-angle contacts against the Tuff of Nugent Wash and the Tuff of Redrock Canyon east of the Benton Spring fault in the northern portion of the field area (Plates 1 and 2). This andesite was also observed on the west side of the Benton Spring fault at the northern end of the fault trace (Plate 1). Clasts of a similar blue-green andesite with large hornblende phenocrysts were observed throughout drainages west of the Benton Spring fault, but no corresponding outcrops were located. Plagioclase from the west side of the fault yielded a weighted mean plateau age of 23.06 ± 0.03 Ma (this study) (Plate 2; Table 1).

Miocene Units

Nonconformably overlying the Blue Sphinx Tuff is a fine-grained white to light gray air-fall tuff interbedded with tuffaceous sandstones and lacustrine deposits (Ms) (Plates 1 and 2). Previous field studies (Ekren and Byers 1984a, 1984b, 1984c, 1984d) indicate that outcrops of similar air-fall tuff interbedded with lacustrine sediments are present throughout the Gabbs Valley Range. Other outcrops of Ms described by Ekren and Byers (1984a, 1984b, 1984c, 1984d) are in depositional contact with the Lavas of Nugent Wash, the Tuff of Nugent Wash, the Tuff of Redrock Canyon, and the Rhyolite of Gabbs Valley Range.

A sequence of lava flows, designated the Lavas of Redrock Canyon, pinches out against the Singatse Tuff and overlies the Lavas of Nugent Wash and the Tuff of Nugent Wash (Plate 1). This sequence, designated the Lavas of Redrock Canyon, consists of three map units: Mrb, Mri, and Mlrr (Plate 2). Unit Mrb is a basaltic andesite which exhibits a dark sheen where locally quenched, typically at the lower exposures of this deposit. Unit Mri, a dacite, is generally found overlying the basaltic andesite. Unit Mlrr is a light grey to dark pink quartz latite (Plate 2). These units were only observed east of the Benton Spring fault.

The Tuff of Redrock Canyon (Mrc) drapes over and frequently pinches out against the Lavas of Nugent Wash, the Tuff of Nugent Wash, the Lavas of Redrock Canyon, and unit Ms (Plate 1). The Tuff of Redrock Canyon grades from rhyodacite at the base to quartz latite in the uppermost portions of the unit (Plate 2). Petrologically, the Tuff of Redrock Canyon is almost identical to the Blue Sphinx Tuff; locally angular granite lithic fragments and fragments of the lavas of Redrock Canyon present in the Tuff of Redrock Canyon allow for distinction. Multiple outcrops of the Tuff of Redrock Canyon preserve cooling columns (Figure 5a). This unit yielded a sanidine $^{40}Ar/^{39}Ar$ age of 22.95 ± 0.04 Ma (this study) (Plate 2; Table 1).

Cross-cutting the Singatse Tuff, the Blue Sphinx Tuff, and the Tuff of Redrock Canyon in various locations throughout the field area is unit Mmi, a series of andesitic dikes (Plates 1 and 2). The three most prominent outcrops of unit Mmi in the field area are found along the Benton Spring fault: the northernmost of the three is located west of the Benton Spring fault and its eastern edge truncates at the fault, the next outcrop to the

south is bounded on both sides by the Benton Spring fault, and the southernmost is located east of the Benton Spring fault and its western edge truncates at the fault. Other outcrops of Mmi were also observed along the contact between the Blue Sphinx Tuff and a younger unit. As outcrops of this unit were observed throughout the field area and no clear contact was identified which could be used as a fault marker, unit Mmi was not used in my evaluation of dextral slip magnitudes. Plagioclase from the northernmost dike yielded a weighted mean plateau age of 22.694 ± 0.102 Ma (this study) (Plate 2; Table 1).

Unconformably overlying the Singatse Tuff and the Blue Sphinx Tuff and post-dating the Tuff of Redrock Canyon is a light grey quartz latite (Mql) (Plate 2). In most outcrops, the majority of the phenocrysts have been replaced with sericite due to apparent hydrothermal alteration. This latite was only observed outcropping west of the Benton Spring fault. Unit Mql yields a plagioclase $^{40}Ar/^{39}Ar$ age of 20.98 ± 0.10 Ma (this study) (Plate 2; Table 1). This age indicates that unit Mql is younger than unit Mrc and thus differentiates Mql from the quartz latite Mlrr east of the Benton Spring fault.

Unconformably overlying the Blue Sphinx Tuff, a light grey andesite lava (Mlo) was only observed in a single outcrop in the northeast portion of the field area (Plates 1 and 2). Mlo is interpreted as a localized lava flow.

In various locales throughout the field area, the Rhyolite of Gabbs Valley Range (Mrl) exhibits intrusive contacts with local rocks as well as localized channelized lava flows (Plate 1). Outcrops of this lava are largely unaltered, unlike most other volcanic units in the field area. Immediately east of the major splay of the Benton Spring fault (Plate 1), a quenched outcrop of the Rhyolite of Gabbs Valley Range was observed; the

proximity to an airfall tuff deposit, which preserves indications of lacustrine deposition, suggests that this flow was deposited in a fluvial or lacustrine environment. Plagioclase from the Rhyolite of Gabbs Valley Range records an $^{40}Ar/^{39}Ar$ age of 20.14 ± 0.26 Ma (this study), making it the youngest dated offset unit in this study (Plate 2; Table 2). Unconformably overlying the Singatse Tuff, the Blue Sphinx Tuff, the Lavas of Nugent Wash, the Tuff of Nugent Wash, the lavas of Redrock Canyon, the Tuff of Redrock Canyon, and the Rhyolite of Gabbs Valley Range are the Lavas of Mount Ferguson (Mlf) (Plates 1 and 2). Mlf consists of a series of lavas ranging from hypersthene andesite to quartz latite that cover much of the eastern edge of the field area (Ekren and Byers, 1984b; this study). Individual flows within the sequence are often separated by light grey air-fall tuff deposits. Cooling columns were frequently observed at various elevations in the Lavas of Mount Ferguson. As this unit generally covers all other outcrops where it is present, it acted as a boundary for eastern extent of the field area. The age of the Lavas of Mount Ferguson has been constrained by multiple studies; hornblende from a basal flow yielded a K/Ar age of 22.5 ± 0.6 Ma (Ekren et al., 1980), $^{40}Ar/^{39}Ar$ geochronology on plagioclase from a flow near the top of Mlf yielded an age of 18.91 ± 0.03 Ma (Lee et al., 2020b), and a K/Ar age of 15.0 ± 0.5 Ma was reported for a plagioclase from one of the youngest flows (Ekren et al., 1980).

Miocene to Quaternary Units

Unit QMb is a dark red to light red tectonite consisting of loose soil interpreted as fault gauge; these deposits were only observed outcropping along the Benton Spring fault (Plates 1 and 2; Figure 8b). The unit is hypothesized to have initially

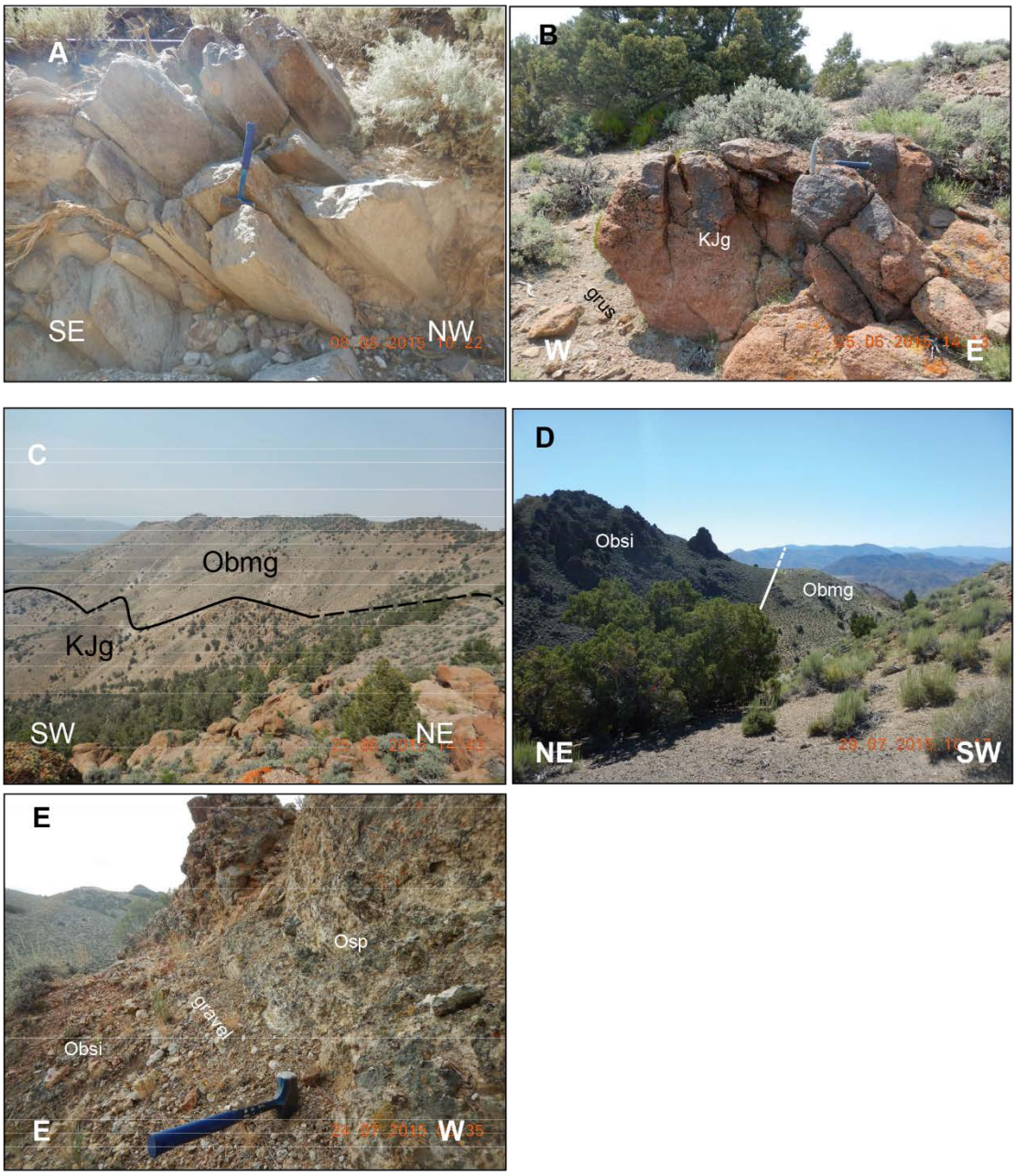

Figure 5. Photographs showing examples of observed features interpreted as evidence of paleovalleys. (A) Cooling columns in Mrc in Wildhorse Canyon, preserving presumed original orientation and displaying non-vertical cooling column formation. (B) Decomposed granite corestone surrounded by grus, representing long-term exposure of unite KJg prior to deposition of Obmg and other Cenozoic tuffs. (C) Exposed contact between KJg and Obmg. (D) Near vertical contact between units Obsi and Obmg which preserves orientation of paleovalley wall. (E) Subhorizontal paleogravel between units Obsi and Osp, indicating that Osp was deposited in an erosional channel within Obsi.

developed cotemporally with initiation of slip along the Benton Spring fault, continuing into the modern. The southernmost exposure of QMb consists of a mélange of unsorted, matrix-supported intrusive and sedimentary breccia clasts ranging from pebbles <5 cm in diameter to outcrops >20 m in diameter. All clasts appear derived from local Mesozoic units. The matrix is comprised of clay and is fault-gouge derived. Other outcrops of Qmb did not contain clasts identifiable as being sourced from specific units from the field area. Qmb outcrops at bends and splays of the Benton Spring fault, with the most prominent example occurring at the major splay in the Benton Spring fault in the Gabbs Valley Range (Plate 1).

Several inactive alluvial fans are preserved throughout the field area; those that have lithified into fanglomerate are designated unit QPfg and are frequently incised by later fluvial features. QPfg is comprised of clasts of Mesozoic, Oligocene, and Miocene units and appears to represent the oldest phase of fan-building preserved in the field area. Non-lithified, inactive alluvial fans are designated QPf. These features are typically located in areas that do not act as modern drainages, but occasionally represent topographic highs that show signs of erosion, rather than fan-building, along modern drainages.

Quaternary Units

Much of the field area in areas of high relief is covered by colluvial sediment (Qc) which obscures older units and contacts. A block of the Lavas of Mount Ferguson was observed downslope from the contact between the Tuff of Redrock Canyon and the Lavas of Mount Ferguson; this block was interpreted as a landslide deposit (Qls).

Unconsolidated alluvial sediments that accumulated outside of the stream beds and channels were mapped as alluvial fan deposits (Qaf). Along the Benton Spring fault as well as elsewhere in the field area, seasonally active stream beds and channels are filled with alluvial sediments (Qa).

$^{40}Ar/^{39}Ar$ Geochronology

To determine emplacement ages for volcanic units within the paleovalleys observed in the Gabbs Valley Range and to allow calculation of fault slip rates based on those ages and the magnitude of offset of associated geologic markers, $^{40}Ar/^{39}Ar$ geochronology samples were collected from five tuffs, lavas, and dikes (units Ola, Mrc, Mmi, Mql, and Mrl in Plates 1 and 2) in the field area. Units Mrc, Mmi, Mql, and Mrl were selected in an effort to determine slip rates along the Benton Spring fault based on three criteria: those units which exhibited paleovalley-style depositional environments, which were observed both east and west of the Benton Spring fault, and recorded dextral offset across the Benton Spring fault. As unit Mmi appears to record two age populations due to the presence of non-atmospheric (Appendix A, Figure A1) and no contact was observed which was consistent both east and west of the Bento Spring fault, the age for unit Mmi was not used in this study. Unit Ola was collected along the Petrified Spring fault and was not used to assess dextral slip across the Benton Spring fault. To collect samples appropriate for $^{40}Ar/^{39}Ar$ dating, minimally-altered outcrops were located within the field area for each unit of interest. A heavy maul was used to remove cobble-sized pieces of each outcrop, which were then broken in the field with standard rock hammers to fragments no more than 5 cm long. Any fragments displaying evidence of weathering

or hydrothermal alteration were discarded, and the process was repeated until between 2 and 3 kilograms of fragments were collected.

Samples were then prepared for $^{40}Ar/^{39}Ar$ analyses at the USGS facility in Menlo Park, CA, under the supervision of Dr. Andrew Calvert. Samples were crushed, washed, and sieved into standard grain sizes: 125-250µm, 250-500µm, 500-1000µm, 1000-1400µm. For samples with abundant feldspars, appropriate size intervals were selected; for samples where fewer grains were recovered, a combined size interval of 125-1000 µm was used. Size intervals were documented for four samples (Table 2). All samples were subsequently washed in an ultrasonic bath; clean groundmass material was then separated via a Frantz magnetic separator at various settings and all feldspars were hand-picked under a binocular microscope. Feldspars were etched with hydrofluoric acid and run through the Frantz magnetic separator again as necessary to remove contaminants. Samples were then given to the staff of Dr. Calvert and analyzed at the USGS TRIGA reactor following the methods described in Appendix A of Nagorsen-Rinke et. al. (2013) using the 27.87 Ma Taylor Creek sanidine as a neutron flux monitor, and ages were then re-calculated based on the 28.4378 Ma Taylor Creek sanidine to make them comparable to the Kuiper et. al. (2008) astronomical age (Appendix A).

TABLE 2. New $^{40}Ar/^{39}Ar$ Geochronology Ages

Unit/Lithology	Map Unit	Sample	Latitude	Longitude	Mineral	Groundmass size interval (μm)	Age ± error (Ma)	Comments
Mafic intrusions	Mmi	BS1	38.73286	-118.31673	plagioclase	1000 - 1400	22.694 ± 0.102	Weighted Mean Plateau Age
Tuff of Red Rock Canyon	Mrc	BS4	38.66201	-118.23448	sanidine	-	22.95 ± 0.04	total fusion age (weighted mean 10 of 10 grains)
Hornblende andesite lava	Ola	BS5	38.72236	-118.30496	plagioclase	-	23.06 ± 0.03	Weighted Mean Plateau Age
Quartz latite flow	Mql	BS6	38.70553	-118.29729	anorthoclase	500 - 1000	20.98 ± 0.10	total fusion age (weighted mean 9 of 10 grains)
Rhyolite of Gabbs Valley Range	Mrl	BS10	38.65639	-118.65639	anorthoclase	250 - 500	20.14 ± 0.26	total fusion age (weighted mean 10 of 10 grains)

Notes: New samples reported herein were irradiated at the U.S. Geological Survey, Denver, Colorado, USA, TRIGA (Training, Research, General Atomics) reactor using the Taylor Creek sanidine at 28.444 Ma (Fleck et al., 2019) as a neutron flux monitor. This standard age is equivalent to the Fish Canyon sanidine age of 28.198 Ma calibrated to the astronomical age of the Melilla tephra (Kuiper et al., 2008). Plateau ages are defined by a consecutive series of steps where ≥50% of 39Ar released is within error. Latitude and longitude recorded in the World Geodetic System 1984.

Ages calculated by
Dr. Andrew Calvert

CHAPTER IV

EVIDENCE FOR PALEOVALLEYS

Previous mapping in the Gabbs Valley Range interpreted unconformable contacts between Mesozoic basement rock and Oligocene and Miocene volcanic units as low-angle normal faults (Hardyman, 1980; Ekren and Byers, 1985 a, b, c, d). Multiple volcanic tuffs with source calderas in central Nevada can be correlated with ash-flow tuff deposits as far west as the Sierra Nevada and these deposits are interpreted as indicating a westward-draining regional network of paleovalleys across the Nevadaplano (e.g. Faulds et. al., 2005; Henry and Faulds, 2010). I hypothesize that the unconformable contacts described in Chapter III instead provide evidence in support of the development of late Mesozoic to early Cenozoic large-scale erosion features in the field area. Paleovalleys in this region are often identified by volcanic and sedimentary rocks unconformably overlying older rock of varying ages and composition, with fluvial gravels often directly underlying the volcanic units (e.g. Faulds et. al., 2005; Henry and Faulds, 2008). Paleovalleys are also identified by the distinctive cross-sectional geometry of the contacts between the infilling units and the basement rock (Henry, 2008). The contacts are typically vertical in some localities and nearly horizontal in others; these contacts are interpreted as the walls and floors of the paleovalleys, respectively (Plate 3). Multiple volcanic units are often confined within a single paleochannel that was incised into the basement rock, and based on my observations described below, I interpret the geometry of the contacts between volcanic units, sedimentary units, and basement rock in the

Benton Spring fault field area as evidence for a history of repeated incision and depositional events (e.g. Henry 2008; Lee et al., 2020b) (Figure 4).

My new mapping and field observations identified five paleovalleys with contacts between the incised and infilling units preserved both east and west of the Benton Spring fault. Each of the five paleovalleys I mapped will hereafter be referred to by the in-filling unit or by the letter designating the location of the contact used as a marker on Plate 1.

Paleovalley A is infilled with the Guild Mine Member of the Mickey Pass Tuff, Obmg (Plates 1 and 3). Obmg is well-documented as a paleovalley-filling ash-flow tuff across the western Basin and Range (Proffett and Proffett, 1976; Ekren and Byers, 1984; Templeton, 1998; Henry, 2008; Lee et al., 2020b). While not observed in the course of my mapping, Proffett and Proffett (1976) reported a Paleogene basal conglomerate marking the base of the Guild Mine Member of the Mickey Pass Tuff in the Singatse Range and Ekberg (2005) report the same basal conglomerate in the Gillis Range. The formation of this conglomerate indicates the fluvial nature of the depositional environment. Within my field area, the southern contact between the Cretaceous-Jurassic granite and the Guild Mine Member of the Mickey Pass Tuff is marked by strongly weathered, decomposed granite, granite core stones, and grus (Figures 5b and 5c). The northern boundary of this paleovalley was not observed and is likely either eroded and covered by younger volcanic units or alluvial deposits (Plate 1). The presence of the grus and paleosol, coupled with the broad U-shaped geometry in cross section of the contact between the Guild Mine Member and the underlying granite (cross-section E in Plate 3),

support the interpretation that the Guild Mine Member of the Mickey Pass Tuff filled a paleovalley developed within Mesozoic basement.

The second paleovalley, Paleovalley B, is infilled with the Singatse Tuff (Plates 1 and 3). The Singatse Tuff is exposed in outcrops in a paleovalley in the Singatse Range (Proffett and Proffett, 1976), ~50 km west of the study area indicating that these tuff-filled paleovalleys traversed the Oligocene surface for at least 10s of kilometers. This tuff exhibits both high- (Figure 5d) and low-angle, conformable and unconformable contacts with the Guild Mine Member of the Mickey Pass Tuff (Plates 1 and 3). These two types of contacts occur in close proximity to one another, with the high-angle contacts locally occurring at higher elevations than the low-angle contacts. No significant paleosol development was observed between the Guild Mine Member and the Singatse Tuff. The high-angle contacts are interpreted as paleovalley walls and the low-angle contacts as the base. I interpret these contacts as being indicative of the U-shaped cross-sectional geometry typical of paleovalleys (cross-section E in Plate 3).

The third paleovalley, Paleovalley C, is infilled with the Blue Sphinx Tuff (Plates 1 and 3). This unit exhibits high-angle contacts with the Singatse Tuff east of the Benton Spring fault and exhibits both low-angle and high-angle contacts west of the Benton Spring fault (Plates 1 and 3). The high-angle contacts west of the Benton Spring fault are largely obscured beneath modern colluvium. A breccia consisting of angular fragments of the Guild Mine Member of the Mickey Pass Tuff and the Singatse Tuff within a dark-colored matrix was observed west of the Benton Spring fault (Figure 5e). A baked contact is present in the uppermost portions of the breccia, which has been heavily

silicified. The Blue Sphinx Tuff is frequently found in direct contact with the Singatse Tuff and is highly friable in those outcrops closest to the contact, suggesting the presence of surficial water at the time of deposition. The evidence in support of a fluvial environment at the time of deposition and the combination of high- and low-angle contacts offers further support that the Blue Sphinx Tuff was deposited in a paleovalley. Due to the presence of younger volcanics which overlie the Blue Sphinx Tuff, the location of the southern paleovalley wall is poorly constrained and is inferred from a single topography-cutting contact between the Singatse Tuff and the Blue Sphinx Tuff (Plate 1).

The fourth paleovalley, Paleovalley D, is filled with the Tuff of Redrock Canyon (Plates 1 and 3). East of the Benton Spring fault, the Tuff of Redrock Canyon was observed both north and south of a local topographic high consisting of the older lavas of Redrock Canyon (Plate 1). The northern contacts of both exposures east of the Benton Spring fault are obscured by younger lava flows from the Rhyolite of Gabbs Valley Range and the Lavas of Mount Ferguson or are in high- and low-angle contact with the older Lavas of Redrock Canyon (Plate 1). The southern contacts with older units for both exposures were observed; for the northern channel the map trace of the contact trends NW-SE, while the map trace of the southern contact trends NE-SW (Plate 1). The northern exposure preserves high-angle contacts between the Tuff of Redrock Canyon and older lava units of Redrock Canyon along the southern contact, which I interpret as evidence that this contact defines a paleovalley wall (Plates 1 and 3). For the southern exposure, contacts with the lavas of Nugent Wash and the Nugent Tuff are shallowly

dipping, implying deposition on a floodplain adjacent to the paleovalley rather than in a paleovalley (Plates 1 and 3). I interpret this distribution of the tuff as evidence that the pyroclastic flow was confined to two separate channels east of the Benton Spring fault (Plate 1). West of the Benton Spring fault, the Tuff of Redrock Canyon displays low- and high-angle contacts atop and adjacent to the Singatse Tuff and Mickey Pass Tuff (Plate 1). The trend of the contact between the Tuff of Redrock Canyon and the older units has a trend of NW-SE. Cooling column intersection lineations in an outcrop of the Tuff of Redrock Canyon yield a Fisher Mean Vector (n = 10) with trend and plunge of 216, 36 (Figure 6) oriented towards the contact between Mrc and Obsi in Wildhorse Canyon. These measurements are interpreted as evidence that west of the Benton Spring fault, the Tuff of Redrock Canyon was deposited against a paleovalley wall which strikes NW and dips 54° NE (Figure 5a).

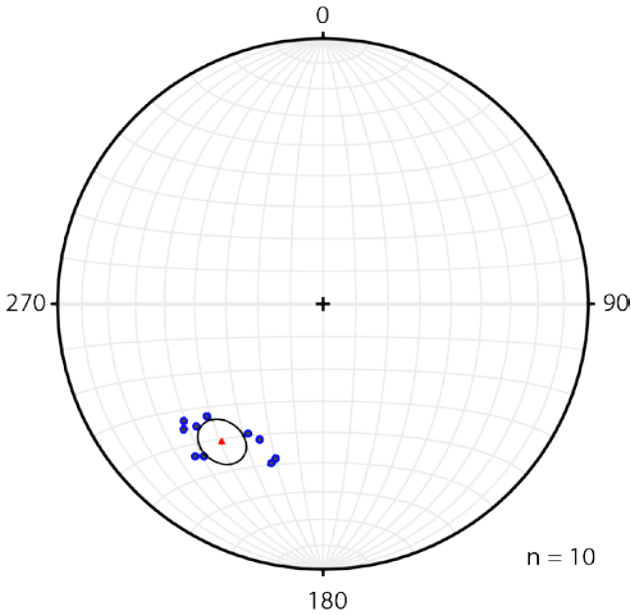

Figure 6. Lower hemisphere, equal area stereonet plot of trend and plunge measurements (blue dots) collected from cooling joint intersections in the Tuff of Redrock Canyon in Wildhorse Canyon. Calculated Fisher mean vector with trend = 216°, plunge = 36° (red triangle indicates mean vector, black ellipse indicates associated error) for measurements (n = 10) shown.

The fifth paleovalley, paleovalley E, is infilled with the Rhyolite of Gabbs Valley Range, unit Mrl (Plates 1 and 3). The Rhyolite of Gabbs Valley Range was observed in contact with the Singatse Tuff, airfall tuff unit Ms, and the Tuff of Redrock

Canyon (Plate 1). Cooling columns intersection lineations within Mrl observed east of the Benton Spring fault exhibited a plunge of 40 degrees, decreasing up-slope to 25 degrees as distance from a local outcrop of the Tuff of Redrock Canyon increased (Figure 7). This type of rosette-style cooling column is common where lava is deposited atop non-horizontal surfaces and indicates that paleovalley incision continued to occur after the deposition of the Tuff of Redrock Canyon. West of the Benton Spring fault, the Rhyolite of Gabbs Valley Range lava unconformably overlies heavily-altered, friable outcrops of the Blue Sphinx Tuff as well as intensely-altered, silicified portions of the Singatse Tuff.

Figure 7. Subhorizontal cooling columns within unit Mrl, indicating deposition against a subvertcal paleovalley wall.

The trends of the paleovalleys range from WNW-ESE to NNW-SSE (Figure 3). The oldest paleovalley, paleovalley A, was incised into the Mesozoic basement rocks of the Gabbs Valley range and reinterpretation of previous mapping suggests that this paleovalley was ~5-km-wide (Plate 1, Figure 3). Subsequent periods of erosion resulted in the development of a series of nested younger paleovalleys that were confined by the initial paleovalley (Plate 1, Figure 3 and Figure 7). Between the deposition of the Singatse Tuff and the Blue Sphinx Tuff, the rapid, near-

linear incision of the paleovalley in the Mesozoic basement appears to have abated; a series of meandering, nested paleovalleys were observed incised in the tuffs of the Benton Spring group (Plate 1, Figure 3 and Figure 7). As such, the trend of a younger paleovalley may vary from its general trend over short distances. The transition from a single major paleovalley to a series of meandering, nested paleovalleys has been previously documented in western Nevada (Faulds et. al., 2005; Henry and Faulds, 2010).

While the southern wall of Paleovalley A is readily identified in the field by the presence of the well-developed paleosol (map unit KPps), the walls of the younger paleovalleys are less well exposed. Several factors contribute to the more limited exposures of the younger paleovalley walls. Modern erosional channels often obscure the contacts, requiring projection of the contact from the few exposed outcrops which preserve surface evidence of the contact. Heavily silicified outcrops were observed near the contact between the Tuff of Redrock Canyon and the Lavas of Mount Ferguson, and extensive alteration of phenocrysts to sericite was observed in thin section for several other units; pervasive alteration may have left these portions of the units more susceptible to erosion. I hypothesize that the older, incised rocks were altered near the contact by the heat of the younger in-filling units in proximity to the contact, and that the silicification observed in these outcrops indicates that alteration occurred concurrent with deposition of the Lavas of Mount Ferguson. Another possible interpretation of localized silicic and sericitic alteration in proximity to these contacts is that the contact acted as a fluid pathway for later hydrothermal fluids.

CHAPTER V

BENTON SPRING FAULT GEOMETRY AND STYLE OF SLIP

The Benton Spring fault is the longest of the four major dextral faults of the eastern Central Walker Lane, followed by the Petrified Spring Fault (e.g. Hardyman 1980; Ekren and Byers 1985a, 1985b, 1986a, 1986b; Lee et al., 2020b). The USGS Quaternary Fault and Fold database lists a total length of 87 km (Sawyer, 1998a). My investigations focus along the central 25 km of Benton Spring fault, representing about 30% of the entire length of the fault.

The Benton Spring fault is a NW-SE striking, near-vertical dextral fault exposed, in part, in the Gabbs Valley Range. The Benton Spring fault is a single through-going fault in most of the field area, with multiple splays along its length (Figure 8A). Exposed fault planes were not observed along the Benton Spring fault. As such, the location of the fault is constrained by the presence of a single linear, well-developed, seasonally active drainage, zones of fault gauge and breccia, and truncated units. In some localities, a well-developed tectonite marks the location of the Benton Spring fault (Figure 8B). Within my field area, the Benton Spring fault has an average strike of 326°, and the relatively linear fault trace cross-cuts topography indicating a dip of ~80-90˚. The Benton Spring fault is largely obscured beneath an active drainage at the northern end of the field area; no fault trace is visible in this drainage. In the south of the field area, the Benton Spring fault bifurcates; the western strand follows the drainage which marks the fault elsewhere in the field area; the eastern strand cross-cuts topography, defines the contact between the Guild

Mine Member of the Mickey Pass Tuff and a Triassic crystalline limestone, and acts as a range-bounding fault further to the southeast.

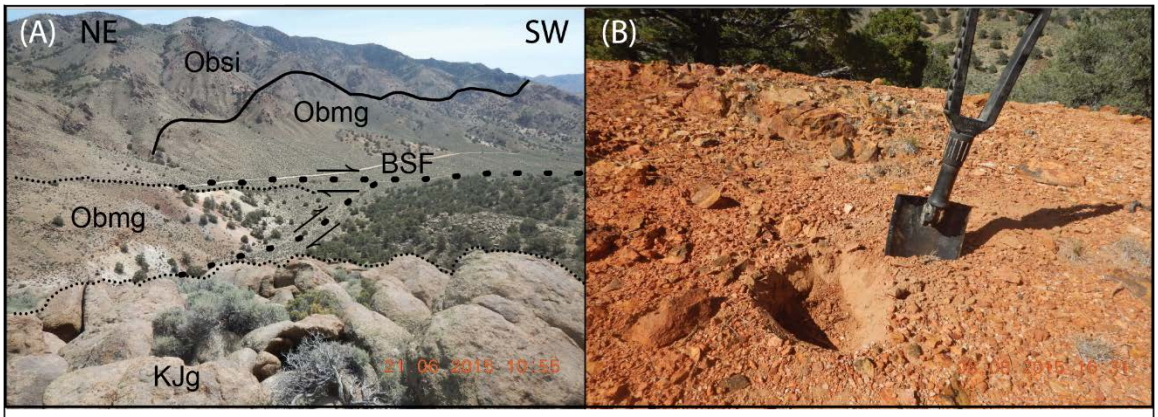

Figure 8. Features of the Benton Spring Fault. (A) View of the Benton Spring Fault (BSF) at the primary southern splay in the field area. KJg in foreground. (B) Well-developed tectonite between two splays of the Benton Spring Fault.

Magnitude of Dextral Offset of Markers

In the field area, the Benton Spring fault cuts all units and offsets the sequence of five nested paleovalleys. In general, the inferred axis of each paleovalley intersects the Benton Spring fault at an angle of 25-35 degrees (Figure 9). Because the southern paleovalley walls are best exposed and are oriented subparallel to the inferred axis of each paleovalley, I use these steeply to near vertical contacts as the markers for measuring the magnitude of dextral offset (Figures 10 and 11). Geological cross-sections were prepared for five transects: cross-sections A, B, and C were prepared to illustrate field relations between units and aid in correlation of proposed paleovalleys, while cross-sections D and E were positioned roughly perpendicular to the proposed paleovalleys to illustrate the interpreted geometry (Plate 3).

The error associated with measured offsets based on the paleovalley walls is determined by the nature of the projection of the paleovalley wall to the Benton Spring fault if the contact does not intersect the fault at the surface, following the method of Lee et al. (2020b) (Figure 10). The uncertainty associated with the magnitude of offset for each paleovalley wall is estimated based on the dip of the paleovalley wall and the distance the contact is projected to the surface expression of the fault. While the walls of the paleovalleys are near-vertical in most cases, like most valley walls there is a shallower slope at the base. As such, while contacts which are not near-vertical may be used to identify a paleovalley wall, significant differences in attitude introduce additional uncertainty due to potential differences in paleoelevation. Three categories of contact projection were defined to determine minimum estimated offset. For offset markers within 100 m of the Benton Spring fault that preserve the high-angle, near-vertical dip of the upper portions of a paleovalley wall, a minimum error of 15% is assigned. When projecting non-vertical contacts over distances greater than 100 m, a minimum error of 30% is assigned. When contacts have been buried by younger units on one side of the fault, a minimum error of 50% is assigned. Error estimates are further refined based on the surface expression of the contacts. For contacts with near-linear map traces, if the strike line orientation of the contact on the east side of the fault is within 5° of the orientation on the west side of the fault, the minimum error is used. Increasing differences in strike line orientation between the expressions of non-horizontals contacts on either side of the fault result in a corresponding increase of error.

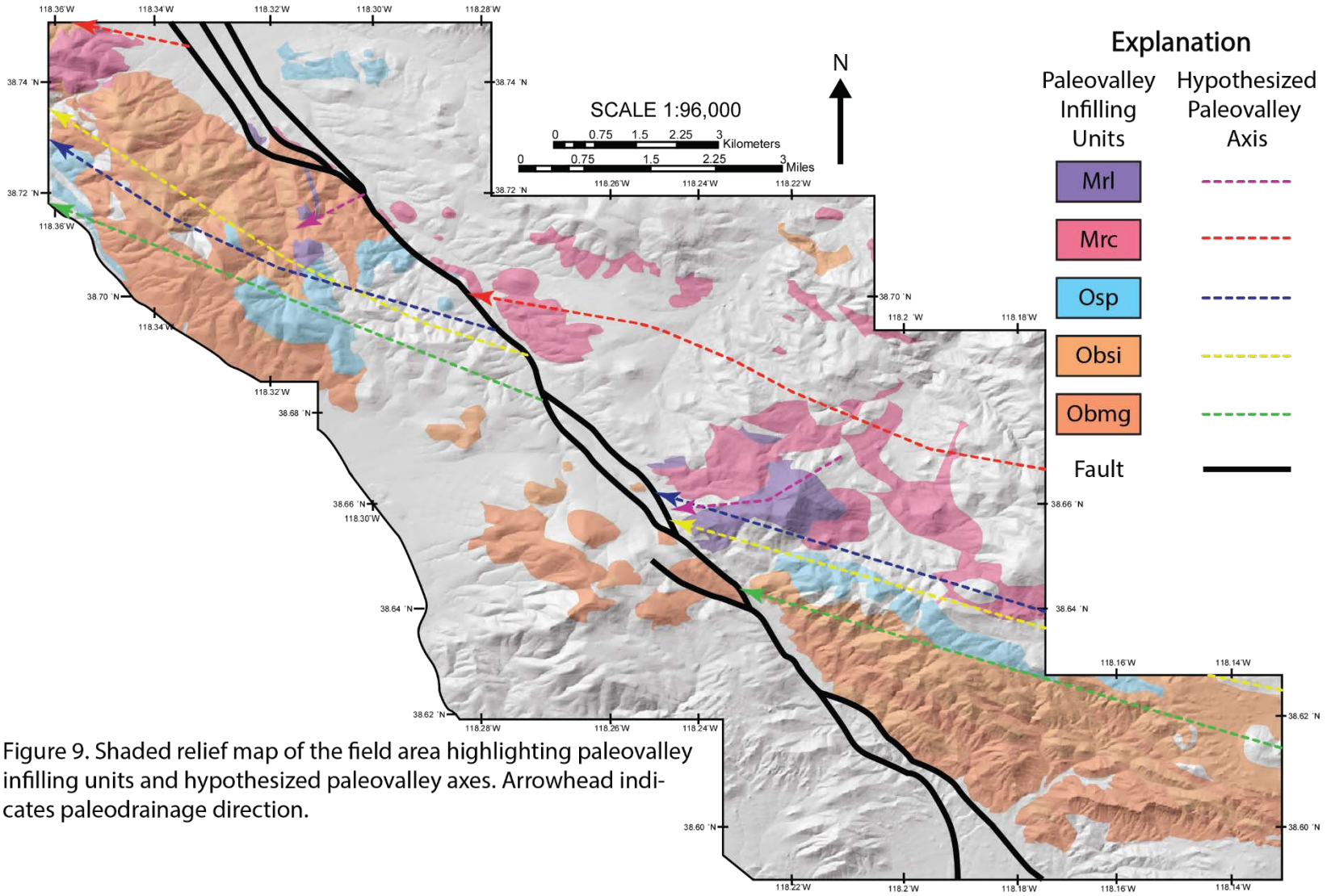

Figure 9. Shaded relief map of the field area highlighting paleovalley infilling units and hypothesized paleovalley axes. Arrowhead indicates paleodrainage direction.

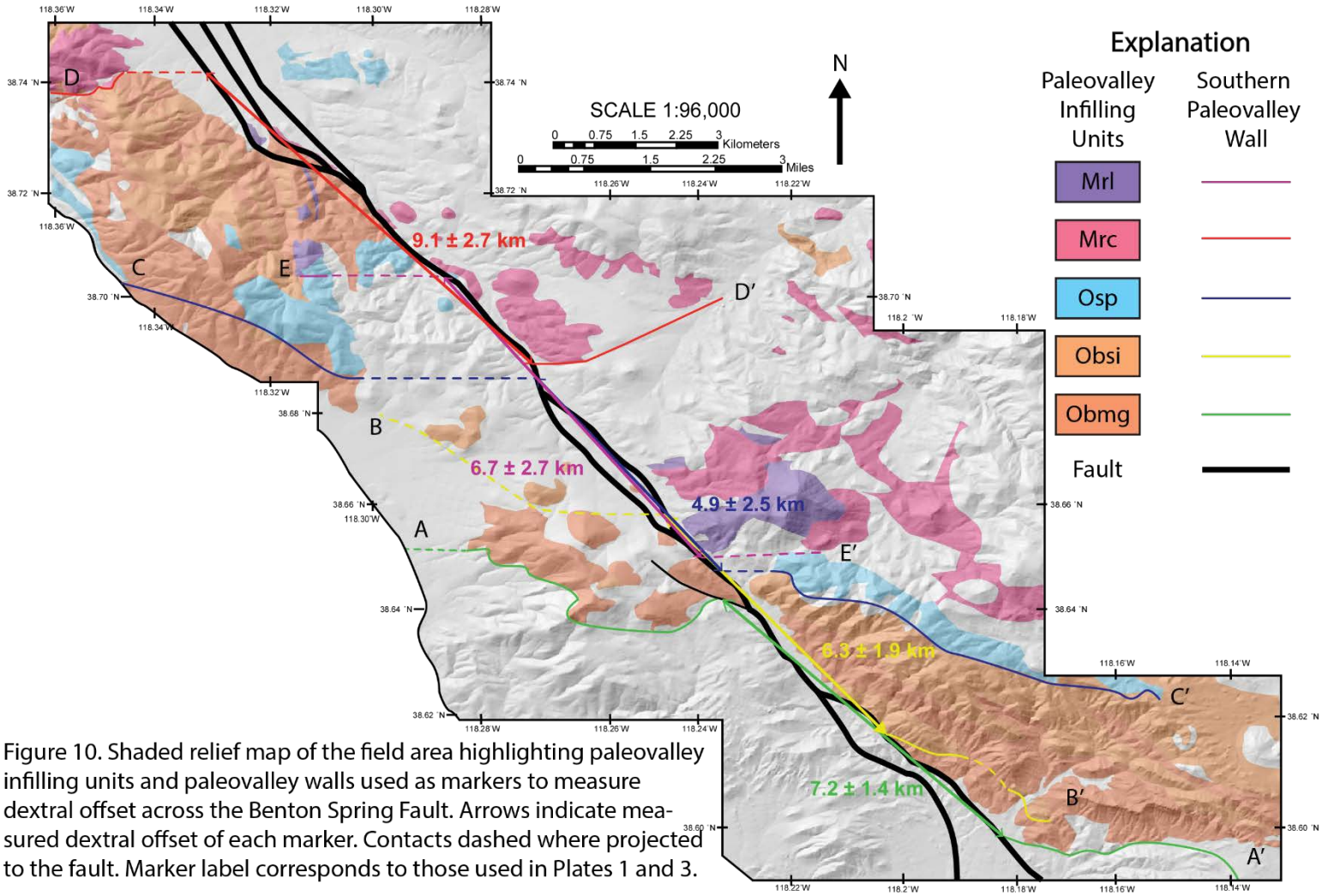

Figure 10. Shaded relief map of the field area highlighting paleovalley infilling units and paleovalley walls used as markers to measure dextral offset across the Benton Spring Fault. Arrows indicate measured dextral offset of each marker. Contacts dashed where projected to the fault. Marker label corresponds to those used in Plates 1 and 3.

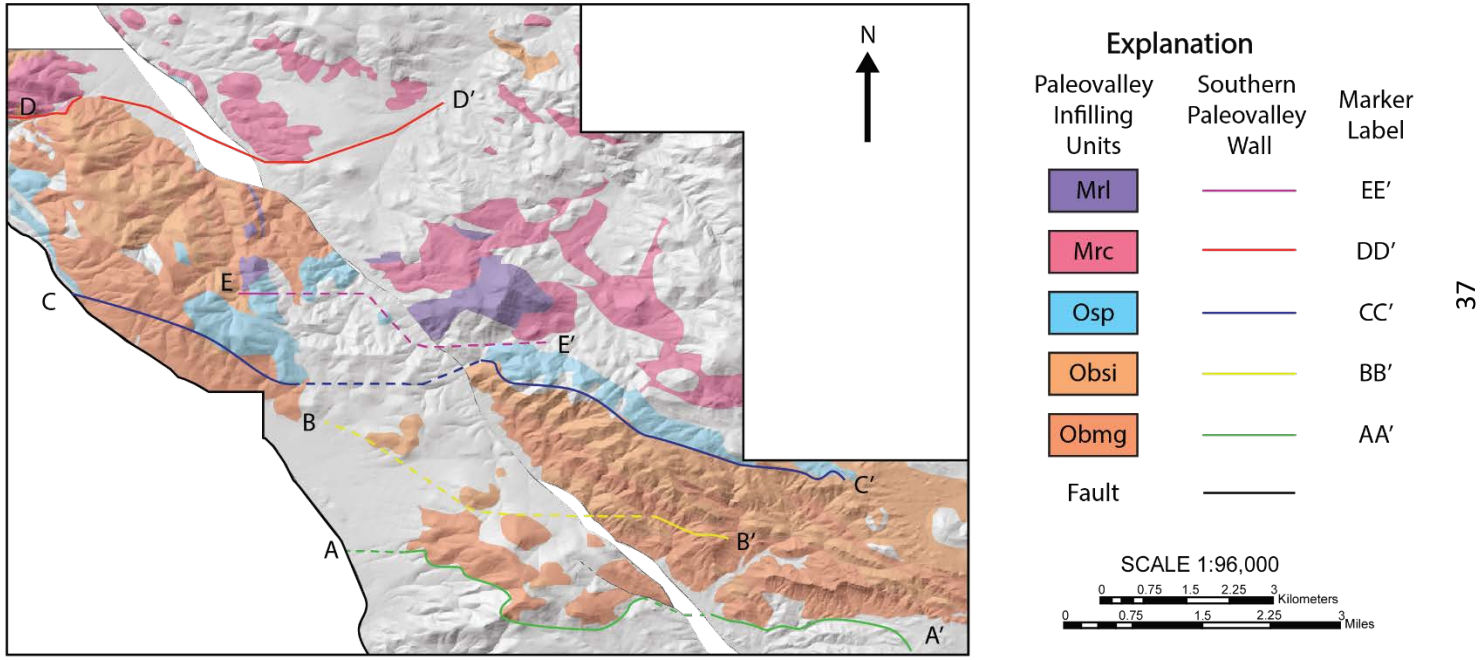

Figure 11. Shaded relief map of the field area highlighting paleovalley infilling units and paleovalley walls used as markers offset across the Benton Spring fault, with offset restored. Portions of map shown in Figure 8 omitted where entrained between fault splays or beyond the northern and southern extents required to show markers. Contacts dashed where projected to the fault. Marker label corresponds to those used in Plates 1 and 3. Average dextral offset is 6.9 ± 1.5 km.

The western exposure of the oldest dextrally offset marker, the southern wall of the Guild Mine Member-filled paleovalley incised into Cretaceous granite, requires the least projection to the fault due to the presence the paleosol in outcrops near the fault (offset marker AA' in Plate 1, green line in Figures 8 and 9). As it is necessary to project the eastern contact approximately 300 m to the Benton Spring fault, I assign a corresponding error of 20% and assess an offset of 7.2 ± 1.4 km.

While excellent exposures of the southern paleovalley wall contact between the Guild Mine Member of the Mickey Pass Tuff and the Singatse Tuff are preserved in contact with the Benton Spring fault on the east side of the fault, west of the Benton Spring fault the southernmost high-angle contact between the two is obscured beneath modern colluvium approximately 1.5 km west of the Benton Spring fault (offset marker BB' in Plate 1; yellow line in Figures 8 and 9). Although both contacts are near vertical, the distance the marker must be projected to the west side of the Benton Spring fault requires assignment of an error of 30%. This contact yields an offset of 6.3 ± 1.9 km when measured relative to a similar contact which intersects the east side of the Benton Spring fault (offset marker BB' in Plate 1; yellow line in Figures 8 and 9).

The Blue Sphinx Tuff-filled southern paleovalley exhibits vertical contacts with the Singatse Tuff on both sides of the Benton Spring fault. The contact west of the Benton Spring fault requires projection ~2.9 km to the fault, as closer to the fault the contact is obscured by overlying younger, strongly altered lavas (offset marker CC' in Plate 1; blue line in Figures 8 and 9). A small (~10 m diameter) outcrop of the Blue Sphinx Tuff is underlain by the same gravel which underlies another outcrop of Blue

Sphinx Tuff further to the north. The presence of this outcrop indicates that the paleovalley in-filled with the Blue Sphinx Tuff can be projected to the Benton Spring fault, although the location of the southern paleovalley wall can only be inferred to be south of this outcrop. East of the Benton Spring fault, the vertical contact between the Blue Sphinx Tuff and the Singatse Tuff is projected approximately 1 km to the fault. The lack of constraints on the location of the paleovalley wall west of the Benton Spring fault and the distance that the paleovalley wall must be projected east of the Benton Spring fault requires a corresponding error of 50%. Projection of the two contacts laterally to the Benton Spring fault yields an offset of 4.9 ± 2.5 km (offset marker CC' in Plate 1; blue line in Figures 8 and 9).

The southern wall of paleovalley D is well preserved west of the Benton Spring fault and is marked by the development of a large drainage, Wildhorse Canyon, along the Tuff of Redrock Canyon-Singatse Tuff contact (offset marker DD' in Plate 1, Red line in Figures 8 and 9). Quaternary alluvial deposits have buried this contact as it approaches the Benton Spring fault from the west, and the contact is projected ~750 m to the Benton Spring fault. It appears that two channels filled with the Tuff of Redrock Canyon are located east of the Benton Spring fault, with a sequence of lavas that both pre- and post-date the emplacement of the Tuff of Redrock Canyon exposed across the ~2 km between the two. The map trace of the shallowly dipping southern wall of the southern channel strikes SW-NE as it approaches the Benton Spring fault, although the intersection of this paleovalley wall and the Benton Spring fault is obscured beneath the Lavas of Mount Fergusson. The map trace of the southern wall of the northern channel preserves a similar

NW-SE orientation to that of Wildhorse Canyon as well as a similar high-angle contact, and as such I conclude that it correlates to the marker west of the fault. As the southern wall of this channel intersects with the Benton Spring fault, the associated error is due solely to projection of the contact west of the Benton Spring fault and an error of 30% is assigned. The northern channel preserves an offset of 9.1 ± 2.7 km (offset marker DD' in Plate 1; red line in Figures 8 and 9).

Paleovalley E, the Rhyolite of Gabbs Valley Range-filled paleovalley, covers significantly less area than the other paleovalley-filling volcanic units in this study and is generally poorly exposed. The assumed southern wall of the Rhyolite of Gabbs Valley Range-filled paleovalley east of the Benton Spring fault is obscured by modern colluvium in one of the sections of the field area where the Benton Spring fault–associated drainage is most steeply incised (offset marker EE' in Plate 1; purple line in Figures 8 and 9). While the contact is obscured by colluvium closer to the fault, the rhyolite is in contact with the Tuff of Redrock Canyon, an older airfall tuff, and the Lavas of Mount Ferguson (Plate 1). West of the Benton Spring fault, the Rhyolite of Gabbs Valley Range is inset into several older tuffs and lavas, including the Guild Mine Member of the Mickey Pass Tuff, the Singatse Tuff, the Blue Sphinx Tuff, and an older quartz latite (Plate 1). The rhyolite is again poorly exposed in this area, but the local sequence of tuffs correlates to those exposed east of the fault. The southern boundary of the rhyolite west of the fault is projected approximately 2 km east to the Benton Spring fault and the southern boundary of the paleovalley east of the fault is in contact with the Benton Spring fault–associated tectonite. Given projection and the obscured contact, an error of 40% is assigned to the

measured offset. An offset of 6.7 ± 2.7 km is assessed based on these two markers and their projections (offset marker EE' in Plate 1; purple line in Figures 8 and 9).

Each measured offset marker records, within error, the same magnitude of dextral offset along the Benton Spring fault (Table 3). Thus, the average dextral offset of the five markers is 6.9 ± 1.5 km (1σ).

TABLE 3. OFFSET MARKERS

Marker Unit	Age (Ma)	Age Source	Dextral Offset (km)
Guild Mine Member of the Mickey Pass Tuff	27.28 ± 0.02	Henry and John (2013)	7.2 ± 1.4
Singatse Tuff	26.85 ± 0.02	Henry and John (2013)	6.3 ± 1.9
Blue Sphinx Tuff	24.30 ± 0.05	Henry and John (2013)	4.9 ± 2.5
Tuff of Redrock Canyon	22.95 ± 0.04	this study	9.1 ± 2.7
Rhyolite of Gabbs Valley Range	20.14 ± 0.26	this study	6.7 ± 3.3

Timing of Offset and Fault Slip Rates

Each of the five markers evaluated in this study record, within error, the same magnitude of dextral offset. As such, I conclude that faulting initiated at some point after emplacement of the youngest offset infilling unit, the Rhyolite of Gabbs Valley Range, at 20.14 ± 0.26 Ma (this study) (offset marker EE' in Plate 1; purple line in Figures 8 and 9). Dividing the average offset of all offset markers of 6.9 ± 1.5 km by the age of the youngest offset marker requires accommodation of uncertainty in both offset and age and yields a minimum dextral slip rate of 0.3 ± 0.2 mm/yr since 20.14 ± 0.26 Ma.

CHAPTER VI

DISCUSSION

Examination of Paleovalley Networks as Fault Marker

This study was centered in part on examination of Cenozoic volcanic units in the field area and determining whether their contacts with the underlying Mesozoic basement rock represented low-angle normal faults, as interpreted by Ekren and Byers (1984, 1985a), or disconformities. Documentation of networks of paleovalleys elsewhere in the Walker Lane (e.g. Henry, 2008; Henry et al., 2012; Lee et al., 2020b; Hoxey et al., 2020) coupled with observations of well-developed corestones and grus along the contacts between Cenozoic volcanic rocks and underlying Mesozoic granites during initial reconnaissance, suggested that at least one paleovalley was present in the Gabbs Valley Range and was offset across the Benton Spring fault. I did not observe fault related rock types and structures, such as fault gauge, slickenlines, visible fault planes, and S-C fabrics, or apparent offset of older horizontal and sub-horizontal contacts across these contacts. Observations of the features detailed as evidence for paleovalleys (see Chapter IV) coupled with the lack of evidence that these contacts are faults confirms that the contacts between Cenozoic and Mesozoic units are depositional nonconformities rather than low-angle faults.

My mapping and structural studies show that paleovalleys record a history of repeated incision and subsequent deposition of infilling volcanic units thus defining a sequence of nested paleovalleys (Figure 7). As previously noted, the distribution of the Tuff of Redrock Canyon indicates that multiple channels were present at the time of

deposition. While the paleovalley walls generally act as reliable offset markers, paleotopographic controls on the development of paleovalleys introduce uncertainty that must be accounted for when utilizing paleovalley walls as fault markers in this region. My use of paleovalleys as fault markers emphasized locating steep paleovalley walls, which are more easily identified in the field than the axis of a paleovalley, as the map traces of these near-vertical features are roughly linear. In addition, the intersection of the near vertical paleovalley walls with near vertical faults define a near vertical line, which is an excellent marker for measuring fault offset.

Benton Spring Fault Slip History

The primary goal of my study was to produce a Oligocene-Miocene fault slip history for the Benton Spring fault. My geologic mapping, geochronology investigations, and collection of structural measurements provide ages and detailed measurements of offset magnitudes for pre-Quaternary Cenozoic fault markers across the Benton Spring fault in the Gabbs Valley Range. Calculations based on the five offset markers yielded an average dextral offset of 6.9 ± 1.5 km; all five markers record similar offset magnitudes when accounting for error. As each of the paleovalleys that I mapped record the same offset, within error, faulting necessarily initiated at some point after the cooling age of the youngest paleovalley filling unit, Mrl, at 20.14 ± 0.26 Ma. Combining the average magnitude of offset for the five markers I documented with the cooling age of the youngest in-filling unit yields a minimum dextral slip rate of 0.3 ± 0.2 mm/yr for the Benton Spring fault in the Gabbs Valley Range.

As offset Miocene and younger markers were not observed, an analysis of the timing of initiation of fault slip and progressive changes in slip rate between the Miocene to present day is not possible with my dataset. However, the adjacent Petrified Springs fault records a history of progressive offset of paleovalleys, whereby Middle Miocene paleovalleys record a larger magnitude of dextral offset and Late Miocene paleovalleys record a smaller magnitude of dextral offset. From these data, Lee et al., (2020b) constrained the initiation of dextral slip along the Petrified Spring fault to between 15.99 ± 0.05 Ma and 15.71 ± 0.03 Ma. If initiation of dextral slip along the Petrified Spring is interpreted as an indication of initiation of dextral slip along all of the major dextral faults of the eastern Central Walker Lane, I calculate an average slip rate of 0.4 ± 0.2 mm/yr for the Benton Spring fault since ~16 Ma. This rate is the same, within error, as the minimum slip rate of 0.4 mm/yr for the Gumdrop Hills fault to the west and the average slip rate of 0.4 ± 0.1 mm/yr for the Petrified Spring fault to the east (Lee et al., 2020b). One possible interpretation of the slip history for the Petrified Spring fault indicates variable slip rates through time (Lee et al., 2020b), thus, it is possible that the Benton Spring fault similarly records variable slip rates.

Multiple studies have examined Pleistocene geologic slip rates along the Benton Spring fault in the Gabbs Valley Range. Langille et al. (2018) utilized U-series and cosmogenic ^{36}Cl geochronology to date alluvial features offset by the Benton Spring fault and calculated offset magnitudes ranging from ~1 m to 70 m. An alluvial fan offset ~31-34 m yielded U-series ages which were the same within error on both sides of the fault (Langille et al., 2018). Utilizing an age of ~13 ka as an estimate for the minimum age of

the fan, a slip rate of ~2-3 mm/yr was calculated for the Benton Spring fault in the Pleistocene (Langille et al., 2018). Another fan was offset ~25-26 m and yielded a cosmogenic ^{36}Cl depth profile age of 10.8 ± 2.5 ka; Langille et al. (2018) calculated a slip rate of ~2-3 mm/yr for this offset fan. Angster et al. (2019) utilized an alluvial fan terrace riser offset 34.5 ± 2.8 m with a ^{10}Be depth profile age of 21.8 $^{+4.1}/_{-0.6}$ ka to calculate a minimum Late Pleistocene slip rate of 1.5 ± 0.2 mm/yr for the Benton Spring fault. These geologic slip rates along the Benton Spring fault are the same, within error, as the 0.98 ± 0.36 mm/yr model GPS slip rate for the Benton Spring fault (Bormann et al., 2016). These rates are higher than both the average slip rate constrained by the youngest offset marker along the Benton Spring fault and the average slip rate calculated with the assumption that slip initiated cotemporally with the Petrified Spring fault.

Comparing Miocene and Pleistocene slip rates further highlights the potential variation in slip rates through time for the Benton Spring Fault. If the minimum 1.5 ± 0.2 mm/yr of slip (Angster et al., 2019) documented along the Benton Spring fault in the Pleistocene represents a consistent slip rate since initiation of dextral slip along the fault, then the average 6.9 ± 1.5 km dextral offset of Cenozoic markers requires that fault slip initiated at ~4.6 Ma. If the late Pleistocene slip rate of 2-3 mm/yr calculated by Langille et al. (2018) represents a consistent slip rate since initiation of dextral slip along the fault, then the average 6.9 ± 1.5 km dextral offset of Cenozoic markers requires that fault slip initiated as late as ~2.3 Ma. Data from the Petrified Spring fault indicates that it may record variable slip rate through time, with an early phase of rapid slip at 1.5 ± 0.5 mm/yr from 16.0 Ma to 11.8 Ma, followed by a slower period of slip at 0.3 ± 0.2 mm/yr from

11.8 Ma to 124 ka, followed by a subsequent acceleration to 0.7 +0.3/-0.2 mm/yr since 124 ka (Lee et al., 2020b). As my data only constrains the maximum initiation of slip along the Benton Spring fault, a similar slip history cannot be calculated for the Benton Spring fault. However, with the assumption that slip along the Benton Spring fault initiated cotemporally with slip along the Petrified Spring fault, the difference between long-term geologic slip rates and Pleistocene geologic and GPS slip rates requires a slip history wherein slip rates across the Benton Spring fault vary through time.

Implications for Regional Fault Kinematics

One of the primary goals of this study was to determine the spatio-temporal distribution of strain across the dextral faults in eastern Central Walker Lane by documenting a fault slip history of the Benton Spring Fault. While the absence of middle Miocene and younger fault markers precluded the development of detailed Neogene slip history for the Benton Spring fault, I determined a maximum initiation age of 20.14 ± 0.26 Ma for dextral slip along the Benton Spring fault. Coupled with the tightly constrained minimum initiation age of 15.71 ± 0.03 Ma for the Petrified Spring fault (Lee et al., 2020b), it is clear that slip in the region initiated or was ongoing in the middle Miocene.

While the slip history of the Petrified Spring fault is the more tightly constrained than the slip histories for the other faults of the eastern Central Walker Lane, Lee et al. (2020b) also calculated slip rates since the Middle Miocene for the Gumdrop Hills fault and Agai Pah Hills fault. The Gumdrop Hills fault is located ~ 4 km west of the Benton Spring fault, while the Agai Pai Hills fault is located ~14 km west of the Benton Spring

TABLE 4. INITIATION AGE AND DEXTRAL OFFSET ALONG FAULTS OF EASTERN CENTRAL WALKER LANE

Fault Name	Maximum dextral slip initiation age	Age source	Average dextral offset (km) of middle Miocene markers	Offset source	Slip rate since middle Miocene
Agai Pah Hills fault	24.30 ± 0.05 Ma	Henry and John (2013)	4.9 ± 1.1	Lee et al. (2020)	0.3 ± 0.1
Indian Head fault	-	Ekren and Byers (1985b)	5.0 ± 0.5	Lee et al. (2020)	-
Radio Tower fault	-	Ekren and Byers (1985b)	0.5 ± 0.05	Lee et al. (2020)	-
Gumdrop Hills fault	22.95 ± 0.04 Ma	Lee et al. (2020)	9.7 ± 1.0	Lee et al. (2020)	0.6 ± 0.1
Benton Spring fault	20.14 ± 0.26 Ma	Lee et al. (2020)	6.9 ± 1.5	This study	0.3 ± 0.1 to 0.4 ± 0.2
Petrified Spring fault	15.99 ± 0.05 Ma	Lee et al. (2020)	9.6 ± 1.1	Lee et al. (2020)	0.5 ± 0.1 to 0.6 ± 0.1

fault (e.g. Ekren and Byers, 1985a, 1985b, 1986a, 1986b). Using the paleovalleys infilled with the Guild Mine Member of the Mickey Pass Tuff and the Blue Sphinx Tuff, as well as the Tuff of Redrock Canyon for the Gumdrop Hills fault, average dextral offset magnitudes of 9.7 ± 1.0 km and 4.9 ± 1.1 km were assessed for the Gumdrop Hills fault and Agai Pah Hills fault, respectively (Lee et al., 2020b) (Table 4). These magnitudes of dextral offset are the same, within error, as the magnitude of dextral offset across the Benton Spring fault. Using the tightly constrained initiation of slip across the Petrified Springs fault and the 9.7 ± 1.0 km average dextral offset of markers across the Gumdrop Hills fault, a slip rate of 0.6 ± 0.1 mm/yr was calculated (Lee et al., 2020b) (Table 4). These slip rates are the same, within error, as the slip rate across the Benton Spring fault if dextral slip initiated in the Middle Miocene. While the magnitude of dextral offset across the Agai Pah Hills fault is less than the minimum magnitude of dextral offset across both the Petrified Spring and Gumdrop Hills faults, the similarities in fault slip magnitude suggest a relatively uniform spatial distribution of slip across the eastern Central Walker Lane. The markers offset across the Agai Pah Hills fault record an average dextral offset of 4.9 ± 1.1 km, and if initiation of dextral slip is constrained to the same time as along the Petrified Spring fault, the Agai Pah Hills fault records a slip rate of 0.3 ± 0.1 mm/yr since the middle Miocene (Lee et al., 2020b) (Table 4). The

similarities in both magnitude of dextral slip and average slip rate since the Middle Miocene suggest that fault slip was distributed roughly uniformly across the dextral faults of the eastern Central Walker Lane.

If dextral slip along all major faults in the eastern Central Walker Lane initiated at ~16 Ma (Lee et al., 2020b), then slip initiated broadly at the same time as normal faulting in the Eastern California Shear Zone and the western Basin and Range (e.g. Miller et al., 1999, Colgan et al., 2010; Lee et al., 2020b). Below, I summarize the timing of normal faulting that is broadly similar to the timing of dextral faulting across the faults that define the eastern CWL (Table 5).

TABLE 5. DOCUMENTED MIDDLE MIOCENE NORMAL FAULT INITIATION AGE WITHIN NORTHERN EASTERN CALIFORNIA SHEAR ZONE AND WESTERN BASIN AND RANGE

Range	Location number[a]	Initation age (Ma)[b]	Reference
East Range	1	17-15	Fosdick and Colgan (2008)
Tobin Range	2	20(?)-14	Gonsior and Dilles (2008)
Shoshone and northern Toiyabe Ranges	3	17-16	Colgan et al. (2008)
Northern Stillwater Range	4	Ca. 14	MacNamee (2015)
Southern Stillwater Range	5	18-14	Colgan et al. (2020)
Verdi Basin	6	Ca. 12	Henry and Perkins (2001)
Gardnerville Basin	7	Middle Miocene (?)	Cashman et al. (2009)
Wassuk Range	8	Ca. 15	Surpless et al. (2002)
Paradise Range	9	22-19[c]	John et al. (1989)
San Antonio Mountains	10	24.0-16.8[c]	Shaver and McWilliams (1987)
Northern White Mountains	11	Ca. 12	Stockli et al. (2003)
Southern Sierra Nevada	12	Ca. 18-12	Lee et al. (2020a)

[a]For location of study areas, see numbers within circles in text Figure 12.

[b]Unless otherwise indicated, age constraints are from low-temperature thermochronology studies of footwall rocks and/or 40Ar/39Ar geochronology on offset volcanics rocks.

[c]K/Ar geochronology on offset volcanic rocks.

Note: adapted from Lee et al. (2020b)

Approximately 130 km northwest of the field area, near Reno, NV, normal slip associated with extension in the Sierra Nevada initiated in the Verdi Basin at ~12 Ma (Henry and Perkins, 2001) (Table 5). Also northwest of the field area, but within 80 km, the Yerington area and Singatse Range record an initiation of extension between 15 and 13 Ma (Dilles and Gans, 1995; Stockli et al., 2002; Surpless et al., 2002). Southeast of the field area, the NE-striking range-bounding normal faults of the Paradise and San Antonio ranges record an initiation of normal slip between 24 and 17 Ma (Shaver and McWilliams, 1987; John et al., 1989) (Table 5).

The Mina Deflection, located south of the field area, is hypothesized to have initiated in the middle Miocene prior to 12 Ma with the formation of a series of ENE-trending half-grabens sealed by a ~12 Ma andesite in the eastern Queen Valley-Montgomery Pass area (Tincher and Stockli, 2009). A second phase of faulting defined by extension along ENE-striking sinistral faults initiated further north between 12 Ma and 3.8 Ma in the Huntoon Mountains (McCosby, 2019). South of the Mina Deflection, range bounding normal faults are documented as recording initiation ages at ~12 Ma along the west flank of the White Mountains (Stockli at al., 2003), at ~16 Ma along the east flank of the Inyo Mountains (Lee et al., 2009), and between 18 and 12 Ma along the Sierra Nevada frontal normal fault (Lee et al., 2020a) (Table 5).

Forces Driving Faulting

Hypotheses that explain the forces that drive deformation across the western U.S. Cordillera must take into account the timing of initiation of slip as well as the geometric and kinematic relations between the dextral faults within the eastern Central Walker Lane

and range-bounding normal faults exposed across the western Basin and Range northern Eastern California Shear Zone (Figure 12). The Benton Spring fault, like the Petrified Spring and Gumdrop Hills faults (Lee et al., 2020b), strikes subparallel to the present-day azimuth of the motion of the Sierra Nevada block relative to the Central Great Basin and to the NW-SE extension of the western Basin and Range (Bennett et al., 2003; Lee et al., 2020b; this study) and strikes roughly perpendicular to the ENE-WSW extension associated with the NNW-SSE-striking normal faults of the northern Eastern California Shear Zone (e.g. Stockli et al., 2003; Lee et al., 2009) (Figure 12).

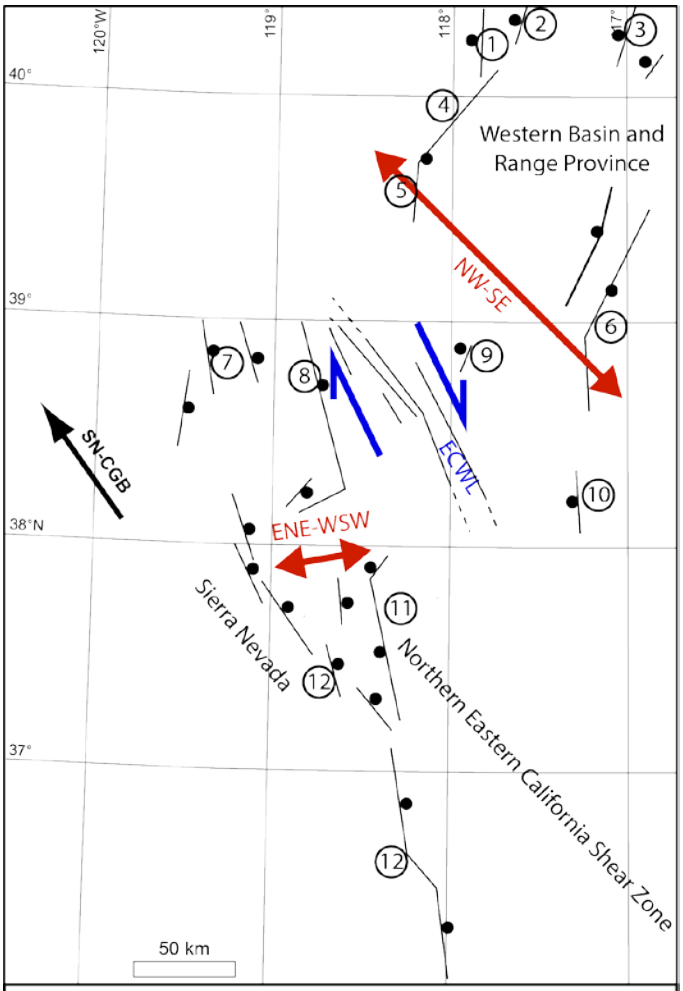

Figure 12. Schematic geometric and kinematic diagram illustrating relationship between the dextral faults of the eastern Central Walker Lane and the normal faults of the Sierra Nevada and Basin and Range in the Middle Miocene. Map shows a simplified version of major normal and dextral faults. Red arrows indicate approximate azimuth of extension, ENE-WSW in the northern Eastern California shear zone and NW-SE in the western Basin and Range. Blue arrows indicate approxmiate NW-SE azimuth of motion across the dextral faults of the eastern Central Walker Lane (ECWL). Black arrow labeled SN-CGB shows present day azimuth of the Sierra Nevada block relative to the Central Great Basin (Bennett et al., 2003). Geographic names are in black. Numbers within circles indicate specific faults used to create simplified fault map; initiation ages for normal faults are listed in Table 5. Fault symbols defined in Figure 2. See text for details.

The similarity in slip initiation timing along and the geometric relationships between the dextral faults of the eastern Central Walker Lane, the normal faults of the northern Eastern California Shear Zone, and the normal faults of the western Basin and Range suggest that slip in the three regions are kinematically related (Figure 12). To accommodate the different Middle Miocene extension directions associated with the normal faults of the northern Eastern California Shear Zone and the western Basin and Range, Lee et al. (2020b) postulated that NW-striking dextral faults of the eastern Central Walker Lane developed as a kinematic link or accommodation zone between the zones of normal faults to the north and south.

While the geometric link between normal faults and dextral faults explains the kinematic origin of the dextral faults in the eastern Central Walker Lane, it does not explain the variable fault slip rates through time along the Petrified Spring fault nor the difference in present-day slip rates along the Benton Spring fault of 1.5 ± 0.2 mm/yr (Bormann et al., 2016; Angster et al., 2019) vs. the minimum 0.3 ± 0.2 mm/yr slip rate since the Middle Miocene (this study). Miocene slip rates are significantly less than Pleistocene and present-day slip rates along both of these faults (e.g. Lee et al., 2020b). An examination of the subduction of the fragments of the Farallon Plate resulting in the lengthening of the Pacific-North American plate boundary, along with the accompanying transition from a subduction to a transform plate boundary, offers a potential explanation for the variable strain rates through time along the dextral faults of the eastern Central Walker Lane (Lee et al., 2020b). The Mendocino Triple Junction marks the point where the plate boundary transitions from subduction to a transform boundary, and the high-

resolution plate boundary reconstructions of DeMets and Merkouriev (2016) indicate that the Mendocino Triple Junction reached the latitude of the field area in the early Pliocene. The slower slip rates along the Benton Spring and Petrified Spring faults thus occurred while the plate boundary at the latitude of the field area was a subduction boundary, the Farallon plate subducting westward beneath the North American plate. The faster rates reported for the Pleistocene and the present-day occurred while the plate boundary was a transform boundary, the Pacific plate moving northwestward relative to the North American plate (e.g. Atwater, 1972; Bormann et al., 2016; Lee et al., 2020b; this study). As such, while the dextral faults of the eastern Central Walker Lane likely developed to accommodate the different directions of extension in the northern Eastern California Shear Zone and the western Basin and Range, modern slip along the faults is driven by the strain associated with the Pacific-North American plate margin (e.g. Dixon et al., 1995; Bennett et al., 2003; Faulds and Henry, 2008; Lee et al., 2009; Delano et al., 2019; Lee et al., 2020b). The dextral faults of the eastern Central Walker Lane are oriented subparallel to the direction of motion associated with the plate boundary, as represented by the azimuth of motion of the Sierra Nevada block relative to the Central Great Basin (Lee et al., 2020b) (Figure 12). This similarity in orientation likely drives the increased slip rates in the eastern Central Walker Lane in the Pleistocene and present-day, as the faults of this region are more ideally oriented to accommodate the strain of the plate boundary slip.

CHAPTER VII

CONCLUSIONS

My new geologic mapping, geochronology, and structural studies document the pre-Quaternary Cenozoic surface expression and dextral slip history along the Benton Spring fault, Gabbs Valley Range, providing context for the spatial-temporal evolution of the major dextral faults of the eastern Central Walker Lane. This study documented tuff- and lava-filled paleovalleys incised into Mesozoic bedrock and other Oligocene and Miocene volcanic units in the Gabbs Valley Range, ages for six of the infilling tuffs and lavas, and the dextral offset magnitudes for five paleovalley markers. Utilizing the offset paleovalley walls observed in the Gabbs Valley Range and the ages calculated for the infilling units, I was able to constrain the maximum age of initiation of dextral slip along the Benton Spring fault. The five markers yield an average dextral offset of 6.9 ± 1.5 km across the Benton Spring fault. The maximum age for initiation of fault slip is 20.14 ± 0.26 Ma, the age of the youngest dextrally offset marker. Combining the average dextral offset yields a minimum dextral slip rate of 0.3 ± 0.1 mm/yr since early Miocene. As the Benton Spring fault shares a similar azimuth, magnitude of dextral offset, and calculated slip rate since the Middle Miocene with the Petrified Spring fault, Agai Pah Hills fault, and the Gumdrop Hills fault, the eastern Central Walker Lane can be confidently said to share a closely linked fault slip history. A Middle Miocene initiation of slip along the Benton Spring fault links the forces which drove slip along this fault in the eastern Central Walker Lane with the forces driving normal faulting throughout the Sierra Nevada and the western Basin and Range. The closely-linked slip histories and apparent

Pliocene increase in slip rate across the dextral faults in the eastern Central Walker Lane indicate that the plate boundary transition from a subduction boundary to a transform boundary caused the slip rate for the Benton Spring fault to vary through time.

REFERENCES

Abe, K., 1981, Magnitudes of large shallow earthquakes from 1904 – 1980, Phys. Earth Planet. Inter., 27, 72 – 92.

Angster, S.J., Wesnousky, S.G., Figueiredo, P.M., Owen, L.A., and Hammer, S.J., 2019, Late Quaternary slip rates for faults of the central Walker Lane (Nevada, USA): Spatiotemporal strain release in a strike-slip fault system, Geosphere, v. 15, p. 1460-1478, doi: 10.1130/GES02088.1.

Argus, G.R.G., 2001, Present tectonic motion across the Coast Ranges and San Andreas fault system in central California: Bulletin of the Geological Society of America, v. 113, p. 1580–1592, doi:10.1130/0016-7606(2001)113<1580:PTMATC>2.0.CO;2.

Armstrong, R.L. and Ward, P., 1991, Evolving geographic patterns of Cenozoic magmatism in the North American Cordillera: The temporal and spatial association of magmatism and metamorphic core complexes: Journal of Geophysical Research, v. 96, p. 13,201–13,224.

Atwater, T., 1970, Implications of plate tectonics for the Cenozoic tectonic evolution of western North America: Bulletin of the Geological Society of America, doi:10.1130/0016-7606(1970)81[3513:IOPTFT]2.0.CO;2.

Atwater, T., 1972, Studies of sea floor spreading and plate movements in the Pacific basin. D. H. Tarling and S. K. Runcorn, ed., Implications of Continental Drift to the Earth Sciences, Vol. 1, Academic Press, p. 213-218.

Atwater, T., and Stock, J.M., 1998, Pacific-North America plate tectonics of the Neogene southwestern United States: An update, International Geology Review, v. 40, p. 375–

402.

Bell, J.W., 1995, Geologic map of the Mina quadrangle, Nevada, Nevada Bureau of Mines and Geology Field Studies Map 10, scale 1:24,000.

Bennett, R.A., Wernicke, B.P., Niemi, N.A., Friedrich, A.M., and Davis, J.L., 2003, Contemporary strain rates in the northern Basin and Range province from GPS data: Tectonics, v. 22, doi: 10.1029/2001TC001355.

Bormann, J.M., Hammond, W.C., Kreemer, C., and Blewitt, G., 2016, Accommodation of missing shear strain in the Central Walker Lane, western North America: Constraints from dense GPS measurements: Earth and Planetary Science Letters, v. 440, p. 169–177, doi:10.1016/j.epsl.2016.01.015.

Carlson, C.W., 2018, Geologic map of the Terrill Mountains quadrangle, Churchill and Mineral counties, Nevada: Nevada Bureau of Mines and Geology Field Studies Map 187, scale 1:24,000.

Cashman, P.H., and Fontaine, S.A., 2000, Strain partitioning in the northern Walker Lane, western Nevada and northeastern California: Tectonophysics, doi:10.1016/S0040-1951(00)00149-9.

Cashman, P.H., Trexler, J.H., Muntean, T.W., Faulds, J.E., Louie, J.N., and Oppliger, G.L., 2009, Neogene tectonic evolution of the Sierra Nevada-Basin and Range transition zone at the latitude of Carson City, Nevada: Special Paper of the Geological Society of America, v. 447, p. 171–188, doi:10.1130/2009.2447(10).

Chapin, C.E., Chamberlin, R.M., Osburn, G.R., and White, D.L., and Sanford, A.R., 1978, Exploration framework of the Socorro geothermal area, Field guide to selected

cauldrons and mining districts of the Datil-Mogollon volcanic field: New Mexico Geological Society Special Publication 7, p. 114–129.

Colgan, J.P., Howard, K.A., Fleck, R.J., and Wooden, J.L., 2010, Rapid middle Miocene extension and unroofing of the southern Ruby Mountains, Nevada: Tectonics, v. 29, TC6022, doi: 10.1029/2009TC002655.

Colgan, J.P., and Henry, C.D., 2009, Rapid middle Miocene collapse of the Mesozoic orogenic plateau in north-central Nevada: International Geology Review, v. 51, p. 920–961, doi: 10.1080/00206810903056731.

Colgan, J.P., Johnstone, S.A., and Shuster, D.L., 2020, Timing of Cenozoic extension in the southern Stillwater Range and Dixie Valley, Nevada: Tectonics, v. 39, no. 3, e2019TC005757, doi: 10.1029/2019TC005757.

Craig, J.W., 2019, Discovery and analysis of a blind geothermal system in the southeastern Gabbs Valley, western Nevada: Geological Society of America Abstracts with Programs, v. 51, paper 94-2, doi: 10.1130/abs/2019AM-337585.

DeCelles, P.G., 2004, Late Jurassic to Eocene evolution of the Cordilleran: American Journal of Science, v. 304, p. 105–168, doi:10.2475/ajs.304.2.105.

DeLano, K., Lee, J., Roper, R., and Calvert, A., 2019, Dextral, normal, and sinistral faulting across the eastern California shear zone-Mina deflection transition, California-Nevada, USA: Geosphere, doi:10.1130/GES01636.1.

DeMets, C., and Dixon, T.H., 1999, New kinematic models for Pacific-North America motion from 3 Ma to present, I: Evidence for steady motion and biases in the NUVEL-1A model: Geophysical Research Letters, doi:10.1029/1999GL900405.

DeMets, C., and Merkouriev, S., 2016, High-resolution reconstructions of Pacific-North America plate motion: 20 Ma to present: Geophysical Journal International, v. 207, p. 741–773, doi:10.1093/gji/ggw305.

Dickinson, W.R., and Wernicke, B.P., 1997, Reconciliation of San Andreas slip discrepancy by a combination of interior basin and range extension and transrotation near the coast: Geology, doi:10.1130/0091-7613(1997)025<0663:ROSASD>2.3.CO;2.

Dickinson, W.R., 2002, The Basin and Range province as a composite extensional domain: International Geology Review, v. 44, p. 1–38, doi: 10.2747/0020-6814.44.1.1.

Dilles, J.H. and Gans, P.B., 1995, The chronology of Cenozoic volcanism and deformation in the Yerington area, western Basin and Range and Walker Lane, Geological Society of America Bulletin, v. 107, p. 474-486.

Dixon, T.H., Robaudo, S., Lee, J., and Reheis, M.C., 1995, Constraints on present-day Basin and Range deformation from space geodesy: Tectonics, v. 14, p. 755–772, doi: 10.1029/95TC00931.

Dixon, T., Farina, F., DeMets, C., Suarez-Vidal, F., Fletcher, J., Marquez-Azua, B., Miller, M., Sanchez, O., and Umhoefer, P., 2000, New kinematic models for Pacific-North America motion from 3 Ma to present, II: Evidence for a “Baja California shear zone”: Geophysical Research Letters, doi:10.1029/2000GL008529.

Dixon, T., Decaix, J., Farina, F., Furlong, K., Malservisi, R., Bennett, R., Suarez-Vidal, F., Fletcher, J., and Lee, J., 2002, Seismic cycle and rheological effects on estimation of present-day slip rates for the Agua Blanca and San Miguel-Vallecitos faults, northern Baja California, Mexico: Journal of Geophysical Research: Solid Earth, v. 107, p. ETG

5-1-ETG 5-23, doi:10.1029/2000jb000099.

Dixon, T.H., Norabuena, E., and Hotaling, L., 2003, Paleoseismology and global positioning system: Earthquake-cycle effects and geodetic versus geologic fault slip rates in the Eastern California shear zone: Geology, doi:10.1130/0091-7613(2003)031<0055:PAGPSE>2.0.CO;2.

Dohrenwend, J.C., 1982, Reconnaissance surficial geologic map of the Gabbs-Luning area, west-central Nevada: U.S. Geological Survey Miscellaneous Field Studies Map MF-1374, scale 1:62,500.

Dohrenwend, J.C., Schell, B.A., Menges, C.M., Moring, B.C., and McKittrick, M.A., 1996, Reconnaissance photogeologic map of young (Quaternary and late Tertiary) faults in Nevada, in Singer, D.A., ed., Analysis of Nevada's metal-bearing mineral resources: Nevada Bureau of Mines and Geology Open-File Report 96-2, 1 pl., scale 1:1,000,000.

Dokka, R.K., and Travis, C.J., 1990, Role of the Eastern California Shear Zone in accommodating Pacific-North American Plate motion: Geophysical Research Letters, doi:10.1029/GL017i009p01323.

Doser, D. I., 1986, Earthquake processes in the Rainbow Mountain-Fairview Peak-Dixie Valley, Nevada, region 1954 – 1959, J. Geophys. Res., 91, 12,572 – 12,586.

Doser, D. I., 1988, Source parameters of earthquakes in the Nevada seismic zone, 1915 – 1943, J. Geophys. Res., 93, 15,001 – 15,015,.

Doubrovine, P. V., and Tarduno, J.A., 2008, A revised kinematic model for the relative motion between Pacific oceanic plates and North America since the Late Cretaceous:

Journal of Geophysical Research: Solid Earth, doi:10.1029/2008JB005585.

Ekren, E.B. and Byers, F.M., Jr., 1984, The Gabbs Valley Range–A well-exposed segment of the Walker Lane in west-central Nevada: in Lintz, Jr., J. ed., Western Geological Excursions Guidebook, Geological Society of American, p. 203-215.

Ekren, E.B. and Byers, F.M., Jr., 1985a, Geologic map of the Gabbs Mountain, Mount Ferguson, Luning, and Sunrise Flat Quadrangles, Mineral County, Nevada, U.S. Geological Survey, Miscellaneous Investigations Series, Map I-1577.

Ekren, E.B. and Byers, F.M., Jr., 1985b, Geologic map of the Win Wan Flat, Kinkaid NW, Kinkaid, and Indian Head Peak Quadrangles, Mineral County, Nevada, U.S. Geological Survey, Miscellaneous Investigations Series, Map I-1578.

Ekren, E.B. and Byers, F.M., Jr., 1986a, Geologic map of the Murphys Well, Pilot Cone, Copper Mountain, and Poinsettia Spring Quadrangles, Mineral County, Nevada, U.S. Geological Survey, Miscellaneous Investigations Series, Map I-1576.

Ekren, E.B. and Byers, F.M., Jr., 1986b, Geologic map of the Mount Annie NW, Mount Annie, Ramsay Spring, and Mount Annie SE Quadrangles, Mineral County, Nevada, U.S. Geological Survey, Miscellaneous Investigations Series, Map I-1579.

Engebretson, D.C., Cox, A., and Gordon, R.G., 1985, Relative Motions between Oceanic and Continental Plates in the Pacific Basin: Geological Society America Special Paper 206, 59 p., doi: 10.1130/SPE206-p1.

Faulds, J.E., Geissman, J.W., and Mawer, C.K., 1990, Structural development of a major extensional accommodation zone in the Basin and Range Province, northwestern Arizona and southern Nevada: Implications for kinematic models of continental

extension, in Wernicke, B.P., ed., Basin and Range Extensional Tectonics near the Latitude of Las Vegas, Nevada: Geological Society of America Memoir 176, p. 37–76, doi:10.1130/MEM176-p37.

Faulds, J.E., Henry, C.D., and Hinz, N.H., 2005, Kinematics of the northern Walker Lane: An incipient transform fault along the Pacific-North American plate boundary: Geology, v. 33, p. 505–508, doi:10.1130/G21274.1.

Faulds, J.E., and Henry, C.D., 2008, Tectonic influences on the spatial and temporal evolution of the Walker Lane : An incipient transform fault along the evolving Pacific – North American plate boundary: Ores and Orogenesis: Circum-Pacific Tectonics, Geologic Evolution, and Ore Deposits: Arizona Geological Society Digest, v. 22, p. 437–470.

Fosdick, J.C., and Colgan, J.P., 2008, Miocene Extension in the East Range, Nevada: A Two-Stage History of Normal Faulting in the Northern Basin and Range: Geological Society of America Bulletin, v. 120, p. 1198–1213, doi:10.1130/B26201.1.

Freymueller, J.T., Murray, M.H., Segall, P., and Castillo, D., 1999, Kinematics of the Pacific-North America Plate Boundary Zone, northern California: Journal of Geophysical Research: Solid Earth, doi:10.1029/1998jb900118.

Gonsior, Z.J., and Dilles, J.H., 2008, Timing and evolution of Cenozoic extensional normal faulting and magmatism in the southern Tobin Range, Nevada: Geosphere, doi:10.1130/ges00137.1.

Gordon, R.G., and Jurdy, D.M., 1986, Cenozoic global plate motions: Journal of Geophysical Research, v. 91, p. 12,389–12,406, doi.org:10.1029/JB091iB12p12389.

Gourmelen, N., and Amelung, F., 2005, Geophysics: Postseismic mantle relaxation in the Central Nevada Seismic Belt: Science, v. 310, p. 1473–1476, doi:10.1126/science.1119798.

Hammond, W.C., Kreemer, C., and Blewitt, G., 2009, Geodetic constraints on contemporary deformation in the northern Walker Lane: 3. Central Nevada seismic belt postseismic relaxation: Special Paper of the Geological Society of America, doi:10.1130/2009.2447(03).

Hammond, W.C., Blewitt, G., and Kreemer, C., 2011, Block modeling of crustal deformation of the northern Walker Lane and Basin and Range from GPS velocities: Journal of Geophysical Research: Solid Earth, v. 116, p. 1–29, doi:10.1029/2010JB007817.

Hardyman, R.F., 1978, Volcanic stratigraphy and structural geology of Gillis Canyon Quadrangle, Northern Gillis Range, Mineral County, Nevada, Reno, Nevada, University of Nevada, Ph.D. thesis, 377 p.

Hardyman, R.F., 1980, Geologic map of the Gillis Canyon Quadrangle, Mineral County, Nevada, U.S. Geological Survey, Miscellaneous Investigations Series, Map I-1237.

Hardyman, R. F., and Oldow, J. S., 1991, Tertiary tectonic framework and Cenozoic history of the central Walker Lane, Nevada, in Raines, G. L., Lisle, R. E., Schafer, R. W., and Wilkinson, W. H., eds., Geology and ore deposits of the Great Basin: Reno, Nevada, Geological Society of Nevada Symposium Proceedings, v. 1, p. 279-301.

Hardyman, R.F., Ekren, E.B., and John, D.A., 2000, Evidence for Cenozoic dextral displacement across the Walker Lane, west central Nevada: Geological Society of

America Abstracts with Programs, v. 32, p. 105.

Hawley, W.B., and Allen, R.M., 2019, The Fragmented Death of the Farallon Plate: Geophysical Research Letters, doi:10.1029/2019GL083437.

Henry, C.D., and Perkins, M.E., 2001, Sierra Nevada–Basin and Range transition near Reno, Nevada: Two-stage development at 12 and 3 Ma: Geology, v. 29, p. 719–722, doi:10.1130/0091-7613(2001)029<0719:SNBART>2.0.CO;2.

Henry, C.D., 2008, Ash-flow tuffs and paleovalleys in northeastern Nevada: Implications for Eocene paleogeography and extension in the Sevier hinterland, northern Great Basin: Geosphere, v. 4, p. 1–35, doi:10.1130/GES00122.1.

Henry, C.D., Hinz, N.H., Faulds, J.E., Colgan, J.P., John, D.A., Brooks, E.R., Cassel, E.J., Garside, L.J., Davis, D.A., and Castor, S.B., 2012, Eocene-early Miocene paleotopography of the Sierra Nevada-Great Basin-Nevadaplano based on widespread ash-flow tuffs and paleovalleys: Geosphere, doi:10.1130/GES00727.1.

Henry, C.D., and John, D.A., 2013, Magmatism, ash-flow tuffs, and calderas of the ignimbrite flareup in the western Nevada volcanic field, Great Basin, USA: Geosphere, v. 9, p. 951–1008, doi:10.1130/GES00867.1.

Hetland, E.A., 2003, Postseismic relaxation across the Central Nevada Seismic Belt: Journal of Geophysical Research, doi:10.1029/2002jb002257.

Hoxey, A., Lee, J., and Calvert, A., 2020, Geologic map of the Petrified Spring fault, Gabbs Valley Range, Mineral County, Nevada: Nevada Bureau of Mines and Geology Open-File Report 20-1, scale 1:24,000, 14 p.

Humphreys, E.D., 1995, Post-Laramide removal of the Farallon slab, western United

States: Geology, v. 23, p. 987–990, doi:10.1130/00917613(1995)023<0987:PLROTF>2.3.CO;2.

Humphreys, E.D., 2009, Relation of flat slab subduction to magmatism and deformation in the western United States, in Kay, S.M., Ramos, V.A., and Dickinson, W.R., eds., Backbone of the Americas: Shallow Subduction, Plateau Uplift, and Ridge and Terrane Collision: Geological Society of America Memoir 204, p. 85–98, doi:10.1130/2009.1204(04).

Humphreys, E.D., and Coblentz, D.D., 2007, North American dynamics and western U.S. tectonics: Reviews of Geophysics, v. 45, RG3001, doi:10.1029/2005RG000181.

John, D.A., Thomason, R.E., and McKee, E.H., 1989, Geology and K-Ar geochronology of the Paradise Peak Mine and the relationship of pre–Basin and Range extension to early Miocene precious metal mineralization in west-central Nevada: Economic Geology and the Bulletin of the Society of Economic Geologists, v. 84, p. 631–649, doi:10.2113/gsecongeo.84.3.631.

Jones, C.H., Farmer, G.L., and Unruh, J.R., 2004, Tectonics of Pliocene removal of lithosphere of the Sierra Nevada, California: Geological Society of America Bulletin, v. 116, p. 1408–1422.

Langille, J., Blisniuk, K., Sharp, W.D., and Lee, J., 2018, Rates of Quaternary dextral slip on the Benton Springs fault, central Walker Lane, western Nevada, constrained through U-series dating of offset alluvial fans, Geological Society of America Abstracts with Programs, v. 50, doi:10.1130/abs/2018RM-313682.

Lechler, A.R., Niemi, N.A., Hren, M.T., and Lohmann, K.C., 2013, Paleoelevation

estimates for the northern and central proto-Basin and Range from carbonate clumped isotope thermometry: Tectonics, doi:10.1002/tect.20016.

Lee, J., Stockli, D.F., Owen, L.A., Finkel, R.C., and Kislitsyn, R., 2009, Exhumation of the Inyo Mountains, California: Implications for the timing of extension along the western boundary of the Basin and Range Province and distribution of dextral fault slip rates across the eastern California shear zone: Tectonics, v. 28, TC1001, doi:10.1029/2008TC002295.

Lee, J., Blythe, A., and Stockli, D., 2020, Miocene slip along the southern Sierra Nevada range front normal fault: Preliminary low-temperature thermochronology results: Geological Society of America Abstracts with Programs, v. 52, no. 4, paper 2-6, doi:10.1130/abs/2020CD -347078.

Lee, J., Hoxey, A.K.R., Calvert, A., and Dubyoski, P., 2020, Plate boundary trench retreat and dextral shear drive intracontinental fault-slip histories: Neogene dextral faulting across the Gabbs Valley and Gillis Ranges, Central Walker Lane, Nevada: Geosphere, v. 16, no. X, p. 1– 27, doi:10.1130/GES02240.1.

Lifton, Z.M., Newman, A.V., Frankel, K.L., Johnson, C.W., and Dixon, T.H., 2013, Insights into distributed plate rates across the Walker Lane from GPS geodesy: Geophysical Research Letters, v. 40, p. 4620–4624, doi:10.1002/grl.50804.

Liu, L., Spasojević, S., and Gurnis, M., 2008, Reconstructing Farallon plate subduction beneath North America back to the Late Cretaceous: Science, doi:10.1126/science.1162921.

MacNamee, A.F., 2015, Thermochronometric investigation of structural evolution and

geothermal systems in extensional settings, Dixie Valley, Nevada [M.S. thesis]: Austin, Texas, University of Texas, 166 p.

McCosby, J.B., 2019, Characterizing the deformation history of the southern Mina Deflection: Field and structural studies in the Huntoon Mountains, California-Nevada [M.S. thesis]: Ellensburg, Washington, Central Washington University, 65 p.

McQuarrie, N., and Oskin, M., 2010, Palinspastic restoration of NAVDat and implications for the origin of magmatism in southwestern North America: Journal of Geophysical Research, v. 115, B10401, doi:10.1029/2009JB006435.

Miller, E.L., Dumitru, T.A., Brown, R.W., and Gans, P.B., 1999, Rapid Miocene slip on the Snake Range-Deep Creek range fault system, east-central Nevada: Geological Society of America Bulletin, v. 111, p. 886–905, doi:10.1130/0016-7606(1999)111<0886:RMSOTS>2.3.CO;2.

Nagorsen-Rinke, S., Lee, J., and Calvert, A., 2013, Pliocene sinistral slip across the Adobe Hills, eastern California-western Nevada: Kinematics of fault slip transfer across the Mina deflection: Geosphere, v. 9, p. 37–53, doi:10.1130/GES00825.1.

Oldow, J.S., and Meinwald, J.N., 1992, Geologic map of the Mina Quadrangle, Nevada Bureau of Mines and Geology Field Studies Map 6, scale 1:24,000.

Oldow, J.S., and Dockery, H.A., 1993, Geologic map of the Bettles Well Quadrangle, Nevada Bureau of Mines and Geology Field Studies Map 1, scale 1:24,000.

Oldow, J.S., Aiken, C.L.V., Hare, J.L., Ferguson, J.F., and Hardyman, R.F., 2001, Active displacement transfer and differential block motion within the central Walker Lane, western Great Basin: Geology, v. 29, p. 19–22, doi:10.1130/0091-

7613(2001)029<0019:ADTADB>2.0.CO;2.

Parsons, T., Thompson, G.A., and Sleep, N.H., 1994, Mantle plume influence on the Neogene uplift and extension of the US western Cordillera? Geology, doi:10.1130/0091-7613(1994)022<0083:MPIOTN>2.3.CO;2.

Petronis, M.S., Zebrowski, P.J., Shields, S.F., Pluhar, C.J., and Lindeman, J.R., 2019, Vertical axis rotation across the eastern Mono Basin and west-central Walker Lane revealed by paleomagnetic data from the Jack Spring tuff: Geochemistry, Geophysics, Geosystems, v. 20, p. 1854–1888, doi:10.1029/2018GC007682.

Proffett, J.M., Jr. and Proffett, B.H., 1976, Stratigraphy of the Tertiary ash-flow tuffs in the Yerington District, Nevada, Nevada Bureau of Mines and Geology, Report 27, 28 p.

Saleeby, J., Le Pourhiet, L., Saleeby, Z., and Gurnis, M., 2012, Epeirogenic transients related to mantle lithosphere removal in the southern Sierra Nevada region, California, part I: Implications of thermomechanical modeling, Geosphere, v. 8, p. 1286–1309, doi:10.1130/GES00746.1.

Saltus, R.W., and Thompson, G.A., 1995, Why is it downhill from Tonopah to Las Vegas?: A case for a mantle plume support of the high northern Basin and Range: Tectonics, v. 14, p. 1235–1244, doi:10.1029/95TC02288.

Savage, J.C., 2004, Strain accumulation across the Coast Ranges at the latitude of San Francisco, 1994–2000: Journal of Geophysical Research, doi:10.1029/2003jb002612.

Sawyer, T.L., and Adams, K.D., compilers, 1998, Fault number 1326, Bettles Well-Petrified Springs fault, in Quaternary fault and fold database of the United States: U.S. Geological Survey website, http://earthquakes.usgs.gov/regional/qfaults, accessed

07/21/2011 01:04 AM.Sawyer, T.L., compiler, 1998, Fault number 1328, Eastern Columbus Salt Marsh fault, in Quaternary fault and fold database of the United States: U.S. Geological Survey website, https://earthquakes.usgs.gov/hazards/qfaults, accessed 08/07/2020 08:38 PM.

Sawyer, T.L., and Adams, K., compilers, 1998, Fault number 1320, Benton Spring fault, in Quaternary fault and fold database of the United States: U.S. Geological Survey website, https://earthquakes.usgs.gov/hazards/qfaults, accessed 08/05/2020 11:26 PM.

Schmandt, B., and Humphreys, E.D., 2011, Seismically imaged relict slab from the 55 Ma Siletzia accretion to the northwest United States: Geology, v. 39, p. 175–178, doi:10.1130/G31558.1.

Shaver, S.A., and McWilliams, M., 1987, Cenozoic extension and tilting recorded in Upper Cretaceous and Tertiary rocks at the Hall molybdenum deposit, northern San Antonio Mountains, Nevada: Geological Society of America Bulletin, v. 99, p. 341–353, doi:10.1130/0016-7606(1987)99<341:CEATRI>2.0.CO;2.

Sonder, L.J., and Jones, C.H., 1999, Western United States extension: How the West was widened: Annual Review of Earth and Planetary Sciences, v. 27, p. 417–462, doi:10.1146/annurev.earth.27.1.417.

Stewart, J.H., 1988, Tectonics of the Walker Lane belt, western Great Basin: Mesozoic and Cenozoic deformation in a zone of shear, in Ernst, W. G., ed., Metamorphism and crustal evolution of the western United States: Prentice Hall, Englewood Cliffs, New Jersey, p. 681-713.

Stockli, D.F., Surpless, B.E., Dumitru, T.A., and Farley, K.A., 2002,

Thermochronological constraints on the timing and magnitude of Miocene and Pliocene extension in the central Wassuk Range, western Nevada: Tectonics, v. 21, p. 10–19, doi.:10.1029/2001TC001295.

Stockli, D.F., Dumitru, T.A., McWilliams, M.O., and Farley, K.A., 2003, Cenozoic tectonic evolution of the White Mountains, California and Nevada: Geological Society of America Bulletin, v. 115, p. 788–816, doi:10.1130/0016-7606(2003)115<0788:CTEOTW>2.0.CO;2.

Surpless, B., Stockli, D.F., Dumitru, T.A., and Miller, E.L., 2002, Two-phase westward encroachment of Basin and Range extension into the northern Sierra Nevada: Tectonics, v. 21, p. 1002–1014, doi:10.1029/2000TC001257.

Templeton, J.H., 1998, Petrology of the Reversely Zoned Mickey Pass Tuff, West-central Nevada: Oregon State University.

Thatcher, W., Foulger, G.R., Julian, B.R., Svarc, J.L., Quilty, E., and Bawden, G.W., 1999, Present-day deformation across the Basin and Range province, western United States: Science, v. 283, p. 1714–1718, doi:10.1126/science.283.5408.1714.

Tincher, C.R., and Stockli, D.F., 2009, Cenozoic volcanism and tectonics in the Queen Valley area, Esmeralda County, western Nevada, in Oldow, J.S., and Cashman, P.H., eds., Late Cenozoic Structure and Evolution of the Great Basin–Sierra Nevada Transition: Geological Society of America Special Paper 447, doi:10.1130/2009.2447(13).

Wang, Y., Forsyth, D.W., Rau, C.J., Carriero, N., Schmandt, B., Gaherty, J.B., and Savage, B., 2013, Fossil slabs attached to unsubducted fragments of the Farallon plate:

Proceedings of the National Academy of Sciences of the United States of America, doi:10.1073/pnas.1214880110.

Wesnousky, S.G., 2005, Active faulting in the Walker Lane: Tectonics, v. 24, p. 1–35, doi:10.1029/2004TC001645.

Wesnousky, S.G., Bormann, J.M., Kreemer, C., Hammond, W.C., and Brune, J.N., 2012, Neotectonics, geodesy, and seismic hazard in the Northern Walker Lane of Western North America: Thirty kilometers of crustal shear and no strike-slip? Earth and Planetary Science Letters, doi:10.1016/j.epsl.2012.02.018.

Wright, H.M.N., Lesti, C., Cas, R.A.F., Porreca, M., Viramonte, J.G., Folkes, C.B., and Giordano, G., 2011, Columnar jointing in vapor-phase-altered, non-welded Cerro Galán Ignimbrite, Paycuqui, Argentina: Bulletin of Volcanology, doi:10.1007/s00445-011-0524-6.

APPENDIXES

APPENDIX D

AGE SUMMARIES

Following the methods outlined in the $^{40}Ar/^{39}Ar$ section of Chapter III, geochronology samples were analyzed and the resulting age data is included in this Appendix. Six samples were dated using $^{40}Ar/^{39}Ar$ incremental heating techniques or a continuous CO_2 laser system; the age data for each sample is comprised of either the age spectrum and isochron or the weighted mean age and isochron. Each age spectrum and isochron data set is comprised of a Cl/K ratio plot, a percent radiogenic material plot, a K/Ca ratio plot, and an apparent age in Ma plot based on cumulative ^{39}Ar released. Weighted mean age and isochron data sets are comprised of a %radiogenic material plot, K/Ca ratio plot, moles of ^{39}K plot, and cumulative probability function plot. Ages for each method are included in the plot for that method. Each of the samples in Table 2 was collected in the Gabbs Valley Range; sample locations are included in Plate 1.

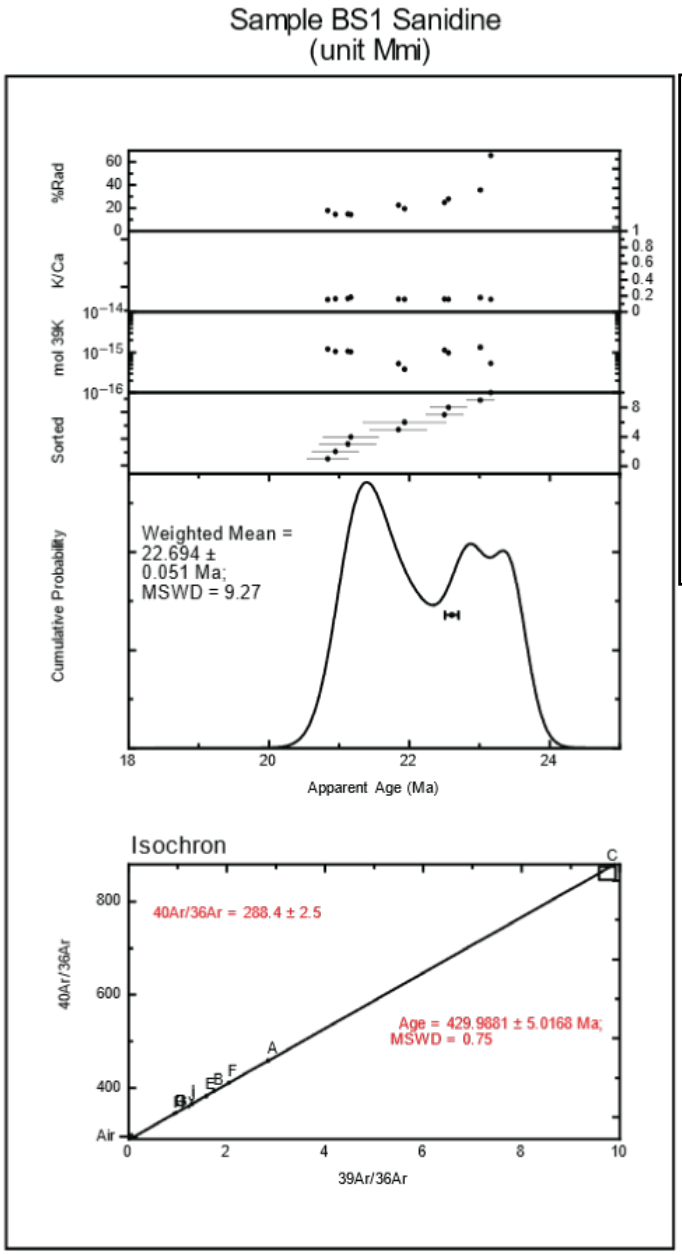

Figure D1. Weighted Mean and Isochron $^{40}Ar/^{39}Ar$ age data for sanidine from Miocene unit Mmi, a mafic dike. Age data is comprised o %Rad plot, K/Ca plot, m ^{39}K plot, Cumulative Probability plot, and $^{40}Ar/^{36}Ar$ vs $^{39}Ar/^{36}Ar$ plot. Summary of ages is shown in Table 2.

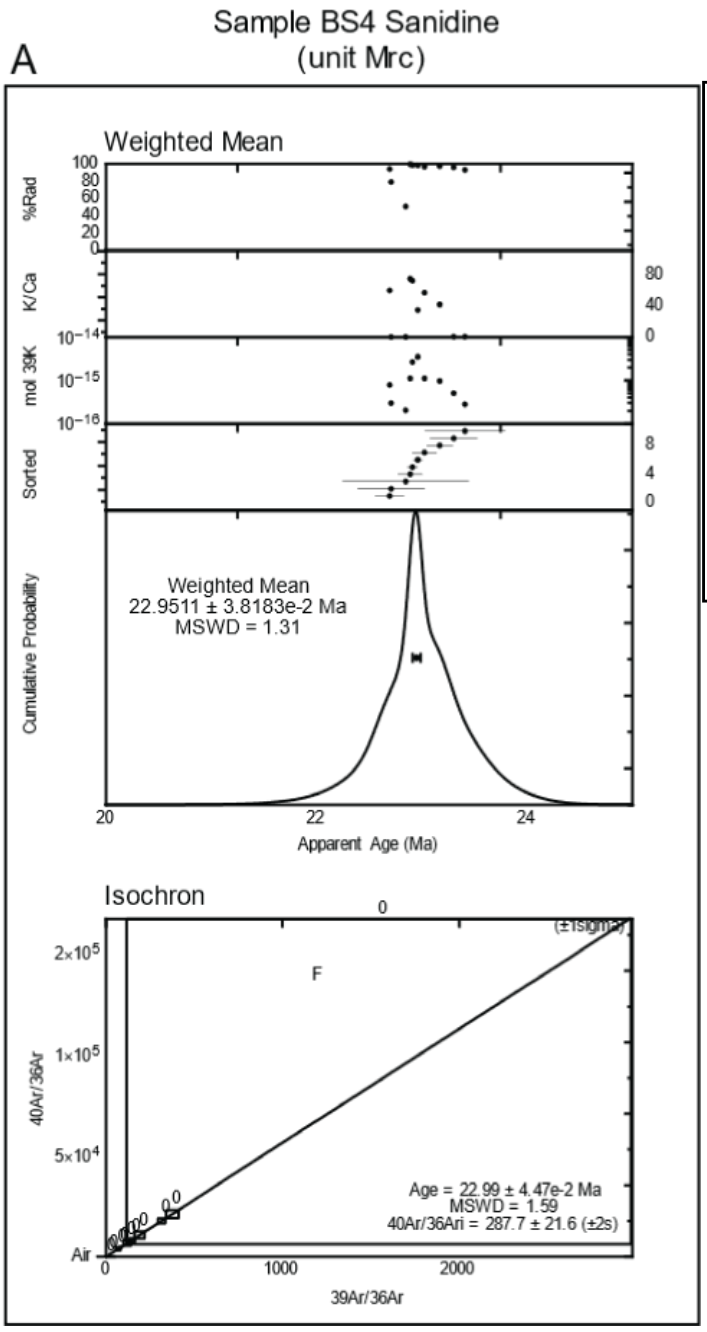

Figure D2. Weighted Mean and Isochron $^{40}Ar/^{39}Ar$ age data for sanidine from Miocene unit Mrc, a rhyodacitic tuff. Age data is co - prised of %Rad plot, K/C plot, mol ^{39}K plot, cumu lative probability plot, and $^{40}Ar/^{36}Ar$ vs $^{39}Ar/^{36}Ar$ plot. Summary of ages i shown in Table 2.

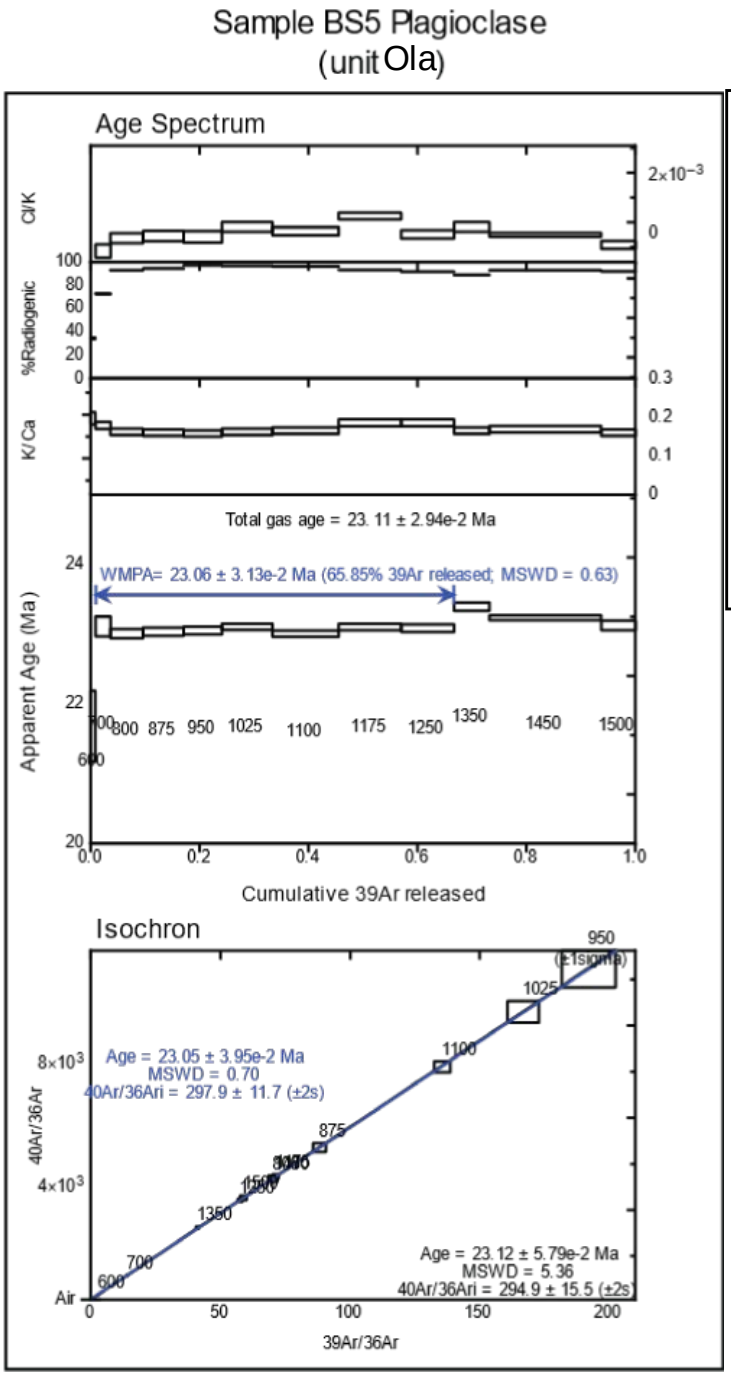

Figure D3. Age Spectrum and Isochron $^{40}Ar/^{39}Ar$ age data for plagioclase from Miocene unit Ola, an andesite lava. Age data is comprised of Cl/K plot, %Radiogenic material plot, K/Ca plot, and apparent age plot, based on cumulative ^{39}Ar released. Summary of ages is shown in Table 2

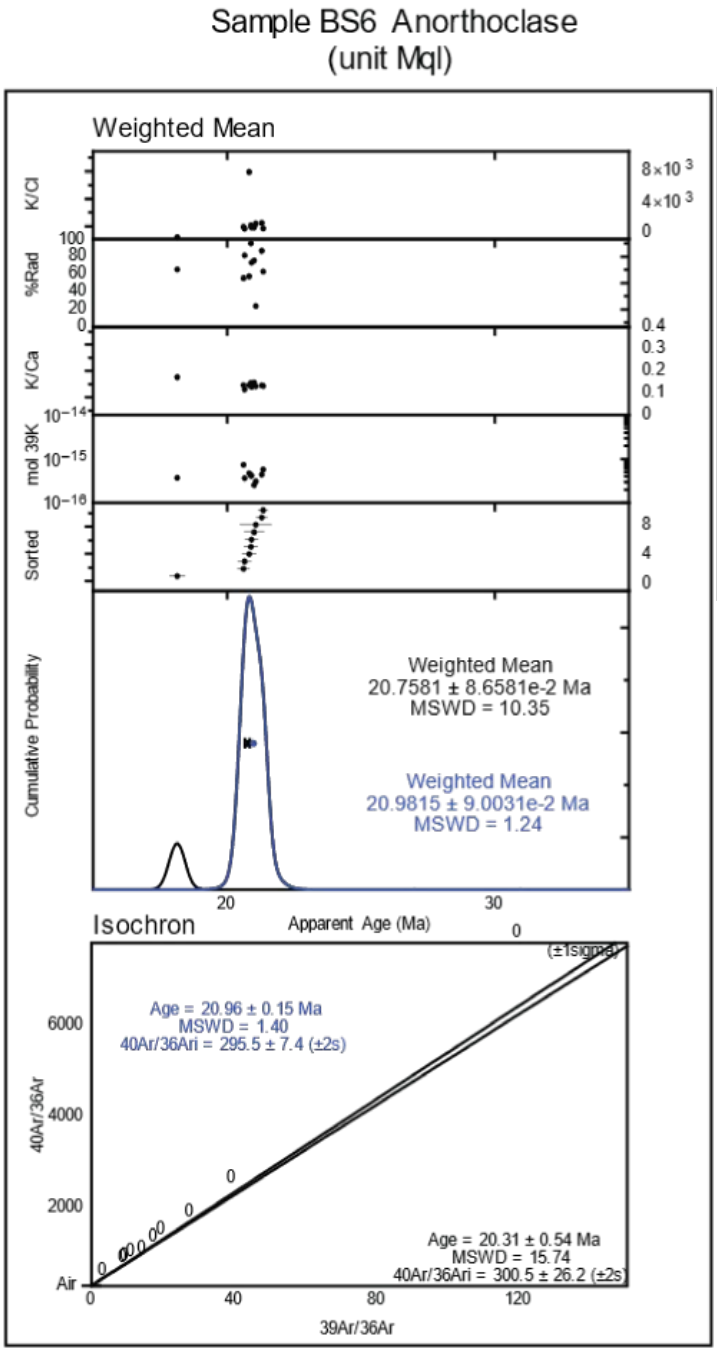

Figure D4. Weighted Mean and Isochron $^{40}Ar/^{39}Ar$ age data for anorthoclase from Miocene unit Mql, a quartz latite lava. Age data is comprised of K/Cl plot, %Rad plot, K/Ca plot, mol 39K plot, and cumulative probability plot. Summary of ages is shown in Table 2.

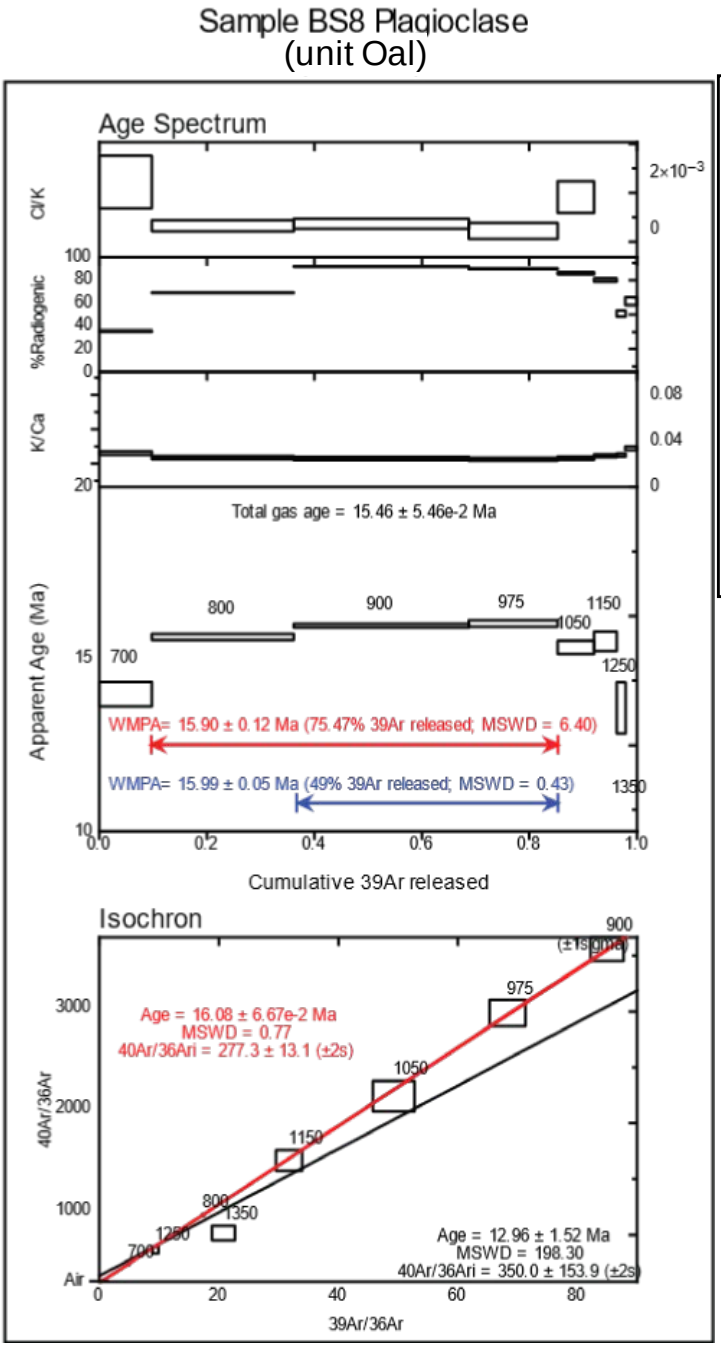

Figure D5. Age Spectru and Isochron $^{40}Ar/^{39}Ar$ age data for plagioclase from Miocene unit Oal, an andesite lava. Age data is comprised of Cl plot, %radiogenic mate al plot, K/Ca plot, and apparent age plot base on cumulative ^{39}Ar released. Summary of ages is shown in Table

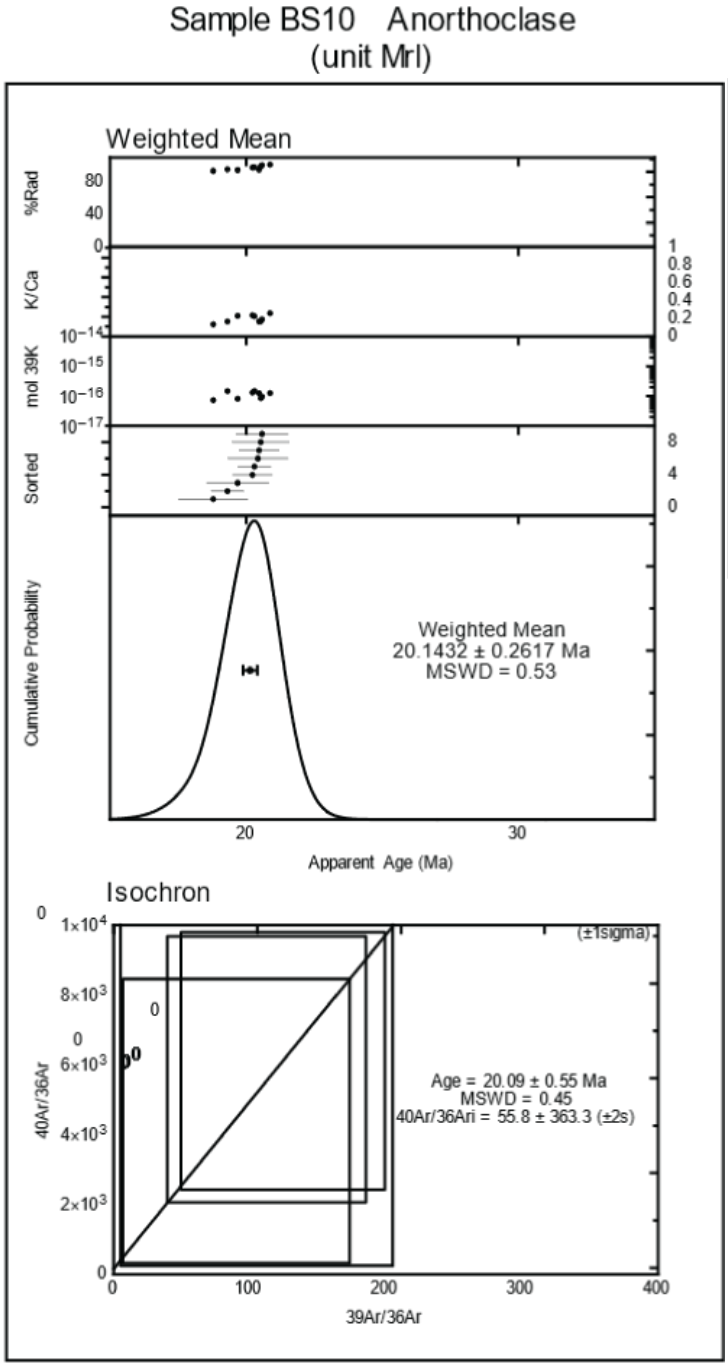

Figure D6. Weighted Mean and Isochron $^{40}Ar/^{39}Ar$ age data for anorthoclase from Miocene unit Mrl, a rhyolite lava. Age data is comprised of %rad plot, K/Ca plot, mol ^{39}K plot, and cumulative probability plot. Summary of ages is shown in Table 2.